# Symplectic tracking through arbitrary magnetic fields

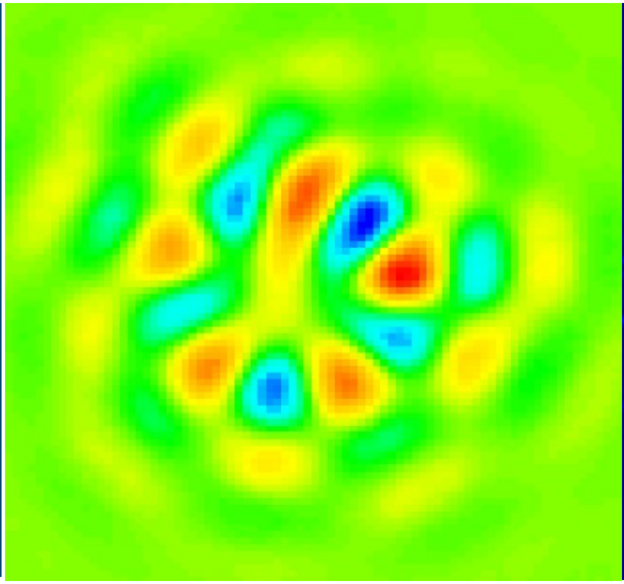


**Ryan Lindberg**

Accelerator Systems Division, Argonne National Laboratory


I.FAST Low Emittance Rings Workshop 2024
CERN, Geneva, Switzerland. February 13th, 2024


Work supported by DOE Contract No. DE-AC02-06CH11357

# Outline and acknowledgments

- Background to symplectic tracking through arbitrary fields
- Our choice to tackle the problem: generalized gradients + implicit integration
- Examples of results using the APS-Upgrade lattice
- Existing challenges for large-angle dipoles and possible solutions
- Conclusions

# Outline and acknowledgments

- Background to symplectic tracking through arbitrary fields
- Our choice to tackle the problem: generalized gradients + implicit integration
- Examples of results using the APS-Upgrade lattice
- Existing challenges for large-angle dipoles and possible solutions
- Conclusions


- Acknowledgments:
  - Michael Borland and Bob Soliday (APS)
  - Marco Venturini (ALS/ALS-U)
  - LCRC Bebop cluster at ANL and weed cluster at ASD

# Choice of symplectic integrator depends upon assumptions

Variation of the magnetic field **B**?

Piece-wise constant

Vector potential $\mathbf{A} = \mathrm{A}_s(x,y)\mathbf{s}$

$H = T(p_x,p_y) + \mathrm{A}_s(x,y)$

Operator splitting yields explicit, symplectic integrators along $s$[1,2] (kick/drift/kick)

[1] E. Forest and R.D. Ruth. "Fourth-order symplectic integration," Physica D **43**, 105 (1990).
[2] H. Yoshida. "Construction of higher order symplectic integrators," Phys. Lett. A **150**, 262 (1990)

# Choice of symplectic integrator depends upon assumptions

An explicit, symplectic integrator for non-canonical coords exists if the numerical representation has $\nabla \cdot \mathbf{B} = 0$ everywhere[3]

Paraxial/small angle approx. + magnetic field **B**

Variation of the magnetic field **B**?

Arbitrary variation

Restrictions to particle motion?

Piece-wise constant

Vector potential $\mathbf{A} = \mathrm{A}_s(x,y)\mathbf{s}$

$H = T(p_x,p_y) + \mathrm{A}_s(x,y)$

Operator splitting yields explicit, symplectic integrators along $s$[1,2] (kick/drift/kick)

[1] E. Forest and R.D. Ruth. “Fourth-order symplectic integration,” Physica D **43**, 105 (1990).
[2] H. Yoshida. “Construction of higher order symplectic integrators,” Phys. Lett. A **150**, 262 (1990)
[3] Y. He, Z.Q. Zhou, Y.J. Sun, J. Liu, and H. Qin. “Explicit K-symplectic algorithms for charged particle dynamics,” Phys. Lett. A **381**, 568 (2017).

# Choice of symplectic integrator depends upon assumptions

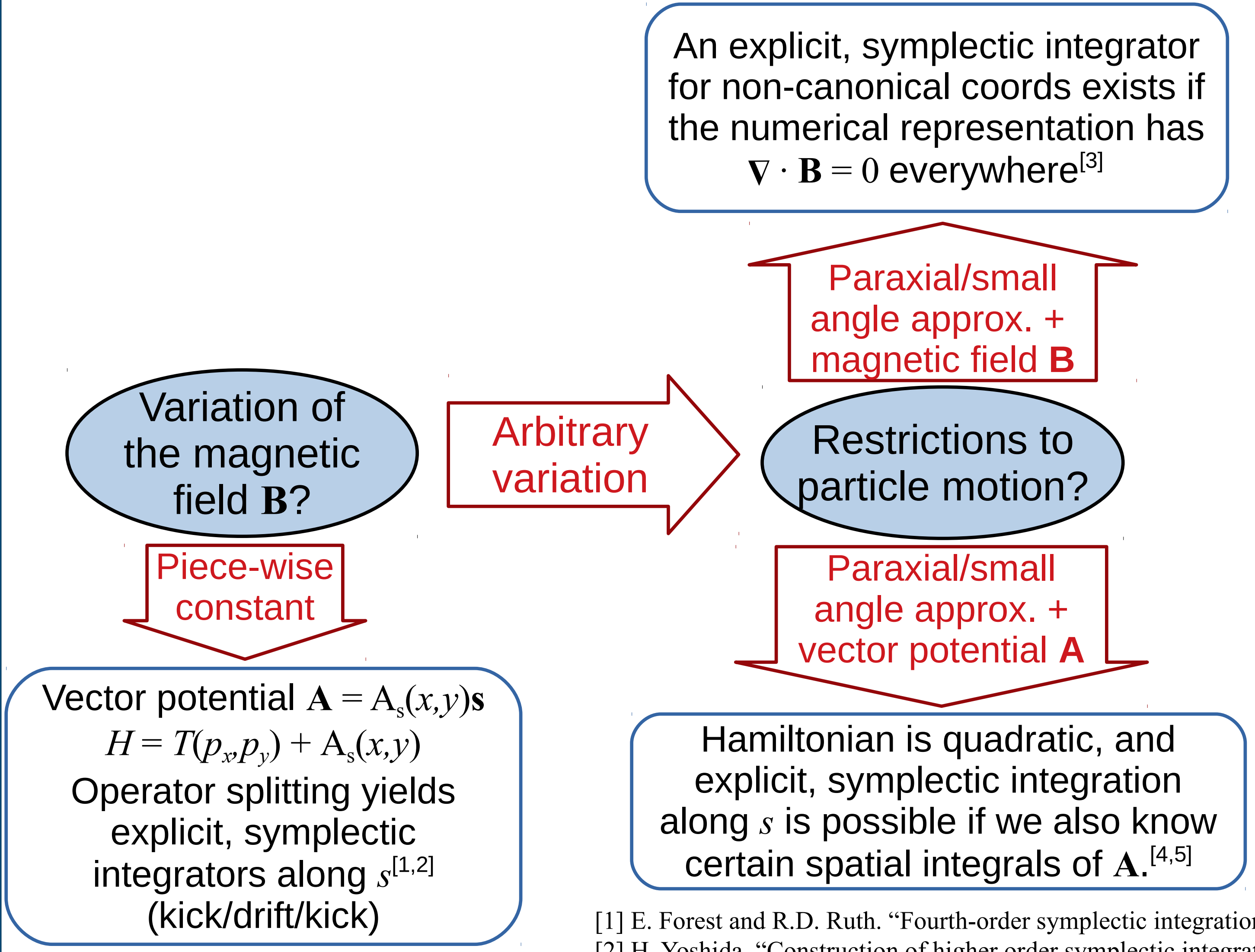


[1] E. Forest and R.D. Ruth. "Fourth-order symplectic integration," Physica D **43**, 105 (1990).
[2] H. Yoshida. "Construction of higher order symplectic integrators," Phys. Lett. A **150**, 262 (1990)
[3] Y. He, Z.Q. Zhou, Y.J. Sun, J. Liu, and H. Qin. "Explicit K-symplectic algorithms for charged particle dynamics," Phys. Lett. A **381**, 568 (2017).
[4] Y. K. Wu, E. Forest, and D. S. Robin. "Explicit symplectic integrator for s-dependent static magnetic field," Phys. Rev. E **68**, 046502 (2003)
[5] A. Wolski and A.T. Herrod, "Explicit symplectic integrator for particle tracking...with curved reference trajectory," PRST-AB **21**, 084001 (2018).

# Choice of symplectic integrator depends upon assumptions

An explicit, symplectic integrator for non-canonical coords exists if the numerical representation has $\nabla \cdot \mathbf{B} = 0$ everywhere[3]

Paraxial/small angle approx. + magnetic field **B**

Variation of the magnetic field **B**?

Arbitrary variation

Restrictions to particle motion?

Arbitrary particle angles

Independent Variable: t or s?

Piece-wise constant

Vector potential $\mathbf{A} = A_s(x,y)\mathbf{s}$

$H = T(p_x,p_y) + A_s(x,y)$

Operator splitting yields explicit, symplectic integrators along $s$[1,2] (kick/drift/kick)

Paraxial/small angle approx. + vector potential **A**

Hamiltonian is quadratic, and explicit, symplectic integration along $s$ is possible if we also know certain spatial integrals of **A**.[4,5]


[1] E. Forest and R.D. Ruth. "Fourth-order symplectic integration," Physica D **43**, 105 (1990).
[2] H. Yoshida. "Construction of higher order symplectic integrators," Phys. Lett. A **150**, 262 (1990)
[3] Y. He, Z.Q. Zhou, Y.J. Sun, J. Liu, and H. Qin. "Explicit K-symplectic algorithms for charged particle dynamics," Phys. Lett. A **381**, 568 (2017).
[4] Y. K. Wu, E. Forest, and D. S. Robin. "Explicit symplectic integrator for s-dependent static magnetic field," Phys. Rev. E **68**, 046502 (2003)
[5] A. Wolski and A.T. Herrod, "Explicit symplectic integrator for particle tracking...with curved reference trajectory," PRST-AB **21**, 084001 (2018).

# Choice of symplectic integrator depends upon assumptions

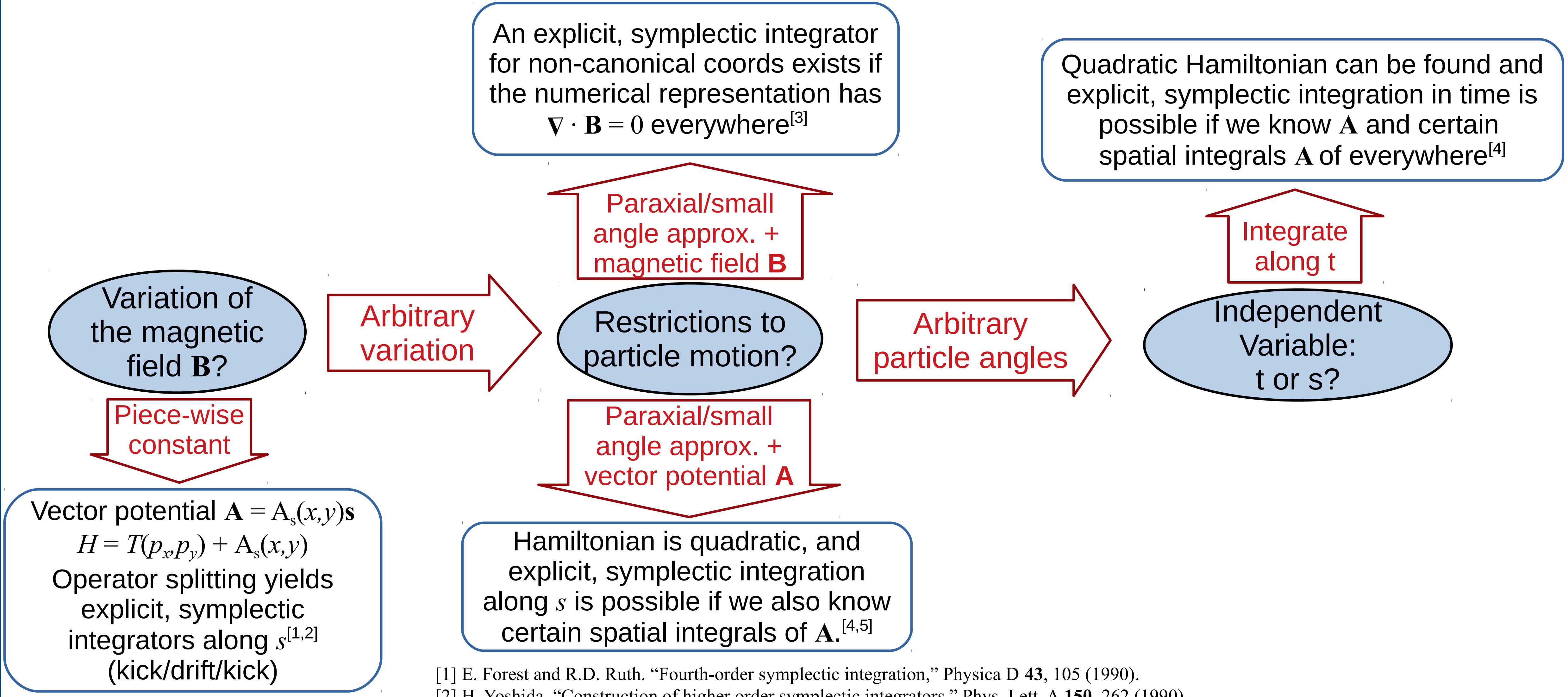


[1] E. Forest and R.D. Ruth. “Fourth-order symplectic integration,” Physica D **43**, 105 (1990).
[2] H. Yoshida. “Construction of higher order symplectic integrators,” Phys. Lett. A **150**, 262 (1990)
[3] Y. He, Z.Q. Zhou, Y.J. Sun, J. Liu, and H. Qin. “Explicit K-symplectic algorithms for charged particle dynamics,” Phys. Lett. A **381**, 568 (2017).
[4] Y. K. Wu, E. Forest, and D. S. Robin. “Explicit symplectic integrator for s-dependent static magnetic field,” Phys. Rev. E **68**, 046502 (2003)
[5] A. Wolski and A.T. Herrod, “Explicit symplectic integrator for particle tracking...with curved reference trajectory,” PRST-AB **21**, 084001 (2018).

# Choice of symplectic integrator depends upon assumptions

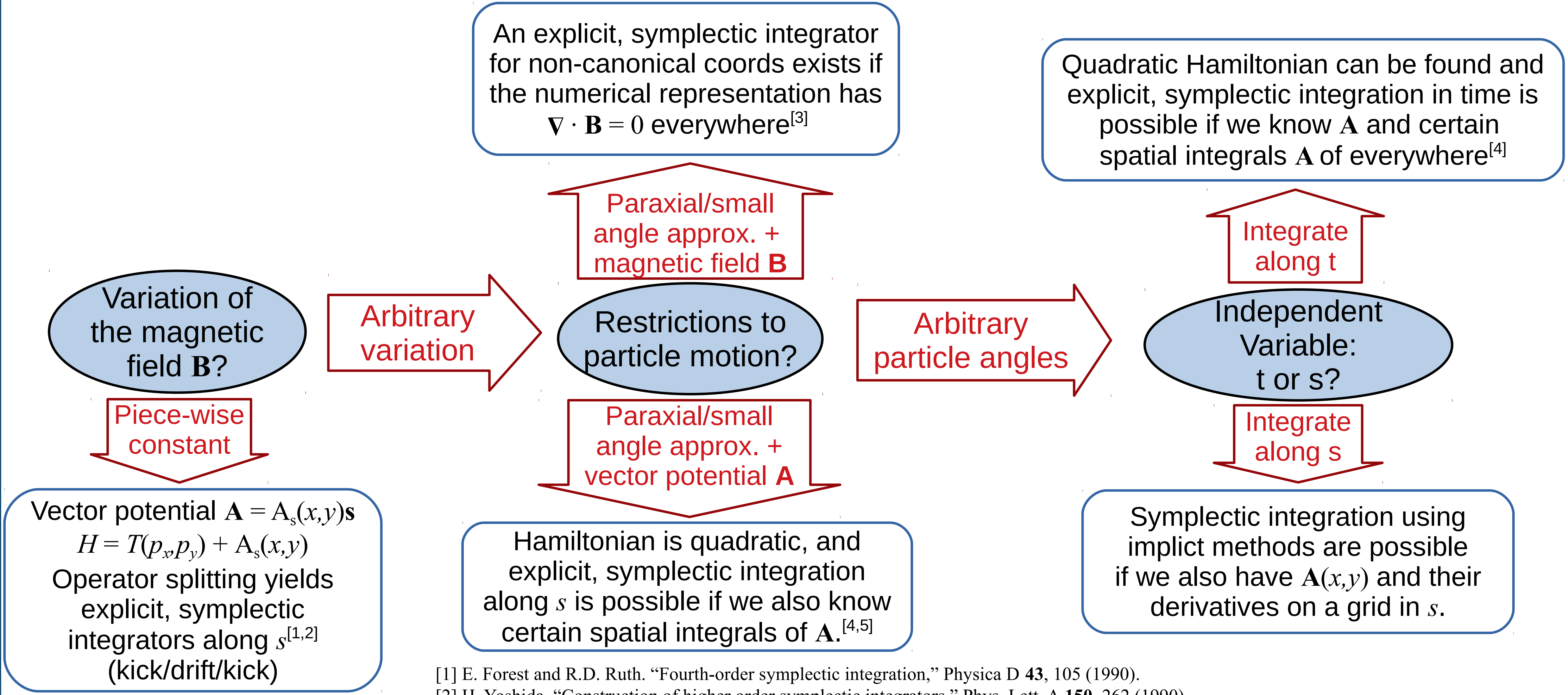


[1] E. Forest and R.D. Ruth. "Fourth-order symplectic integration," Physica D **43**, 105 (1990).
[2] H. Yoshida. "Construction of higher order symplectic integrators," Phys. Lett. A **150**, 262 (1990)
[3] Y. He, Z.Q. Zhou, Y.J. Sun, J. Liu, and H. Qin. "Explicit K-symplectic algorithms for charged particle dynamics," Phys. Lett. A **381**, 568 (2017).
[4] Y. K. Wu, E. Forest, and D. S. Robin. "Explicit symplectic integrator for s-dependent static magnetic field," Phys. Rev. E **68**, 046502 (2003)
[5] A. Wolski and A.T. Herrod, "Explicit symplectic integrator for particle tracking...with curved reference trajectory," PRST-AB **21**, 084001 (2018).

# Our choice for symplectic integration

- We track particles using (symplectic) implicit midpoint method

$$\boldsymbol{x}_{n+1} = \boldsymbol{x}_n + \Delta s \frac{\partial}{\partial \boldsymbol{p}} \mathcal{H}\left[\tfrac{1}{2}(\boldsymbol{x}_{n+1} + \boldsymbol{x}_n), \tfrac{1}{2}(\boldsymbol{p}_{n+1} + \boldsymbol{p}_n); s + \tfrac{1}{2}\Delta s\right]$$

$$\boldsymbol{p}_{n+1} = \boldsymbol{p}_n - \Delta s \frac{\partial}{\partial \boldsymbol{x}} \mathcal{H}\left[\tfrac{1}{2}(\boldsymbol{x}_{n+1} + \boldsymbol{x}_n), \tfrac{1}{2}(\boldsymbol{p}_{n+1} + \boldsymbol{p}_n); s + \tfrac{1}{2}\Delta s\right]$$

using the single particle Hamiltonian in Cartesian coordinates

$$\mathcal{H} = \sqrt{(1+\delta)^2 - [p_x - a_x(x, y; s)]^2 - [p_y - a_y(x, y; s)]^2} - a_z(x, y; s)$$

# Our choice for symplectic integration

- We track particles using (symplectic) implicit midpoint method

$$\boldsymbol{x}_{n+1} = \boldsymbol{x}_n + \Delta s \frac{\partial}{\partial \boldsymbol{p}} \mathcal{H}\left[\tfrac{1}{2}(\boldsymbol{x}_{n+1} + \boldsymbol{x}_n), \tfrac{1}{2}(\boldsymbol{p}_{n+1} + \boldsymbol{p}_n); s + \tfrac{1}{2}\Delta s\right]$$

$$\boldsymbol{p}_{n+1} = \boldsymbol{p}_n - \Delta s \frac{\partial}{\partial \boldsymbol{x}} \mathcal{H}\left[\tfrac{1}{2}(\boldsymbol{x}_{n+1} + \boldsymbol{x}_n), \tfrac{1}{2}(\boldsymbol{p}_{n+1} + \boldsymbol{p}_n); s + \tfrac{1}{2}\Delta s\right]$$

using the single particle Hamiltonian in Cartesian coordinates

$$\mathcal{H} = \sqrt{(1+\delta)^2 - [p_x - a_x(x,y;s)]^2 - [p_y - a_y(x,y;s)]^2} - a_z(x,y;s)$$

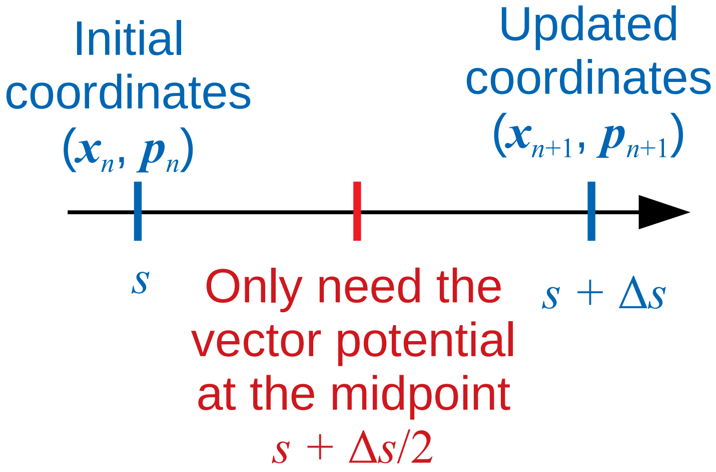


- Tracking requires a numerical representation of the vector potential $\mathbf{A}(x,y;s_n+\Delta s/2)$ and its derivatives

# Our choice for symplectic integration

- We track particles using (symplectic) implicit midpoint method

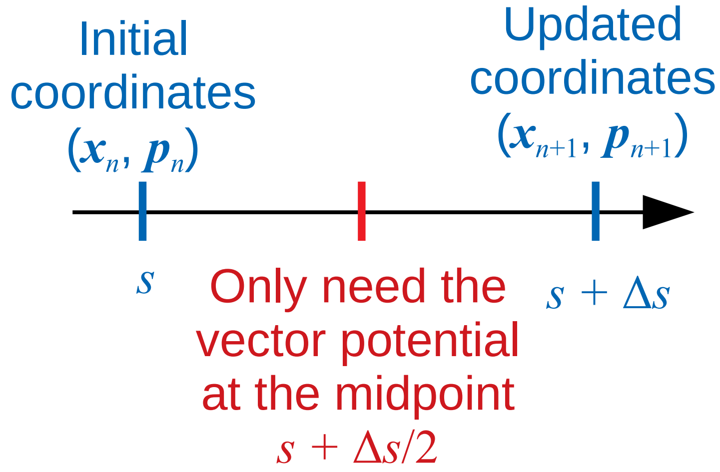


$$\boldsymbol{x}_{n+1} = \boldsymbol{x}_n + \Delta s \frac{\partial}{\partial \boldsymbol{p}} \mathcal{H}\left[\tfrac{1}{2}(\boldsymbol{x}_{n+1} + \boldsymbol{x}_n), \tfrac{1}{2}(\boldsymbol{p}_{n+1} + \boldsymbol{p}_n); s + \tfrac{1}{2}\Delta s\right]$$

$$\boldsymbol{p}_{n+1} = \boldsymbol{p}_n - \Delta s \frac{\partial}{\partial \boldsymbol{x}} \mathcal{H}\left[\tfrac{1}{2}(\boldsymbol{x}_{n+1} + \boldsymbol{x}_n), \tfrac{1}{2}(\boldsymbol{p}_{n+1} + \boldsymbol{p}_n); s + \tfrac{1}{2}\Delta s\right]$$

using the single particle Hamiltonian in Cartesian coordinates

$$\mathcal{H} = \sqrt{(1+\delta)^2 - [p_x - a_x(x, y; s)]^2 - [p_y - a_y(x, y; s)]^2} - a_z(x, y; s)$$

- Tracking requires a numerical representation of the vector potential $\mathbf{A}(x,y;s_n+\Delta s/2)$ and its derivatives
- We choose to represent the fields using the generalized gradient expansion
  - The fields $\mathbf{A}$ and $\mathbf{B}$ are expressed using a generalized power series in the transverse coordinates
  - The coefficients are located at discrete $z$ (or $s$), and describe $z$-dependent “multipoles” and derivatives:

$$A_z = -xC_1(z) - (x^2 - y^2)C_2(z) - (x^3 - 3xy^2)C_3(z) + \tfrac{3}{8}(x^3 + xy^2)C_1''(z) + \ldots + \text{Skew terms}$$

Dipole     Quadrupole     Sextupole

# Generalized gradients are an attractive field representation

- A. Dragt and colleagues developed the generalized gradient representation for accelerator tracking[6,7,8]

$$A_z = -xC_1(z) - (x^2 - y^2)C_2(z) - (x^3 - 3xy^2)C_3(z) + \frac{3}{8}(x^3 + xy^2)C_1''(z) + \ldots + \text{Skew terms}$$

Dipole Quadrupole Sextupole

$$B_r = \sum_{m=1}^{\infty}\sum_{\ell=0}^{\infty} \frac{(-1)^\ell m!(2\ell+m)}{4^\ell \ell!(\ell+m)!} r^{2\ell+m-1}\left\{C_{m,s}^{[2\ell]}(z)\sin(m\phi) + C_{m,c}^{[2\ell]}(z)\cos(m\phi)\right\} + \sum_{\ell=1}^{\infty}\frac{(-1)^\ell 2\ell}{4^\ell \ell!\ell!} r^{2\ell-1} C_{0,c}^{[2\ell]}(z)$$

$$B_\phi = \sum_{m=1}^{\infty}\sum_{\ell=0}^{\infty} \frac{(-1)^\ell m!\, m}{4^\ell \ell!(\ell+m)!} r^{2\ell+m-1}\left\{C_{m,s}^{[2\ell]}(z)\cos(m\phi) - C_{m,c}^{[2\ell]}(z)\sin(m\phi)\right\} \quad B_z = \sum_{m=0}^{\infty}\sum_{\ell=0}^{\infty} \frac{(-1)^\ell m!}{4^\ell \ell!(\ell+m)!} r^{2\ell+m}\left\{C_{m,s}^{[2\ell+1]}(z)\sin(m\phi) + C_{m,c}^{[2\ell+1]}(z)\cos(m\phi)\right\}$$


[6] M. Venturini and A. Dragt. "Accurate computation of transfer maps from magnetic field data," Nucl. Instrum. Methods Res. A **427**, 387 (1999).
[7] A. J. Dragt. *Lie Methods for Nonlinear Dynamics with Applications to Accelerator Physics*. Univ. of Maryland, College Park, 2020.
[8] C. E. Mitchell. "Calculation of Realistic charged-particle transfer maps." PhD thesis, University of Maryland, College Park (2007).

# Generalized gradients are an attractive field representation

- A. Dragt and colleagues developed the generalized gradient representation for accelerator tracking[6,7,8]

$$A_z = -xC_1(z) - (x^2 - y^2)C_2(z) - (x^3 - 3xy^2)C_3(z) + \frac{3}{8}(x^3 + xy^2)C_1''(z) + \ldots + \text{Skew terms}$$

Dipole Quadrupole Sextupole

$$B_r = \sum_{m=1}^{\infty}\sum_{\ell=0}^{\infty} \frac{(-1)^\ell m!(2\ell+m)}{4^\ell \ell!(\ell+m)!} r^{2\ell+m-1}\left\{C_{m,s}^{[2\ell]}(z)\sin(m\phi) + C_{m,c}^{[2\ell]}(z)\cos(m\phi)\right\} + \sum_{\ell=1}^{\infty}\frac{(-1)^\ell 2\ell}{4^\ell \ell!\ell!} r^{2\ell-1} C_{0,c}^{[2\ell]}(z)$$

$$B_\phi = \sum_{m=1}^{\infty}\sum_{\ell=0}^{\infty} \frac{(-1)^\ell m!\, m}{4^\ell \ell!(\ell+m)!} r^{2\ell+m-1}\left\{C_{m,s}^{[2\ell]}(z)\cos(m\phi) - C_{m,c}^{[2\ell]}(z)\sin(m\phi)\right\} \quad B_z = \sum_{m=0}^{\infty}\sum_{\ell=0}^{\infty} \frac{(-1)^\ell m!}{4^\ell \ell!(\ell+m)!} r^{2\ell+m}\left\{C_{m,s}^{[2\ell+1]}(z)\sin(m\phi) + C_{m,c}^{[2\ell+1]}(z)\cos(m\phi)\right\}$$

- The generalized gradient representation enjoys a number of nice properties
  - Provides an analytic expression of $\mathbf{A}$ on planes of constant $z$ → Symplectic tracking is possible
  - The equation $\nabla\cdot\mathbf{B} = 0$, while $\nabla\times\mathbf{B} = 0$ to a high order in the particle coordinates on planes of constant $z$.


[6] M. Venturini and A. Dragt. “Accurate computation of transfer maps from magnetic field data,” Nucl. Instrum. Methods Res. A **427**, 387 (1999).
[7] A. J. Dragt. *Lie Methods for Nonlinear Dynamics with Applications to Accelerator Physics*. Univ. of Maryland, College Park, 2020.
[8] C. E. Mitchell. “Calculation of Realistic charged-particle transfer maps.” PhD thesis, University of Maryland, College Park (2007).

# Generalized gradients are an attractive field representation

- A. Dragt and colleagues developed the generalized gradient representation for accelerator tracking[6,7,8]

$$A_z = -xC_1(z) - (x^2 - y^2)C_2(z) - (x^3 - 3xy^2)C_3(z) + \frac{3}{8}(x^3 + xy^2)C_1''(z) + \ldots + \text{Skew terms}$$

Dipole   Quadrupole   Sextupole

$$B_r = \sum_{m=1}^{\infty}\sum_{\ell=0}^{\infty} \frac{(-1)^\ell m!(2\ell+m)}{4^\ell \ell!(\ell+m)!} r^{2\ell+m-1} \left\{C_{m,s}^{[2\ell]}(z)\sin(m\phi) + C_{m,c}^{[2\ell]}(z)\cos(m\phi)\right\} + \sum_{\ell=1}^{\infty} \frac{(-1)^\ell 2\ell}{4^\ell \ell!\ell!} r^{2\ell-1} C_{0,c}^{[2\ell]}(z)$$

$$B_\phi = \sum_{m=1}^{\infty}\sum_{\ell=0}^{\infty} \frac{(-1)^\ell m!\, m}{4^\ell \ell!(\ell+m)!} r^{2\ell+m-1} \left\{C_{m,s}^{[2\ell]}(z)\cos(m\phi) - C_{m,c}^{[2\ell]}(z)\sin(m\phi)\right\} \quad B_z = \sum_{m=0}^{\infty}\sum_{\ell=0}^{\infty} \frac{(-1)^\ell m!}{4^\ell \ell!(\ell+m)!} r^{2\ell+m} \left\{C_{m,s}^{[2\ell+1]}(z)\sin(m\phi) + C_{m,c}^{[2\ell+1]}(z)\cos(m\phi)\right\}$$

- The generalized gradient representation enjoys a number of nice properties
  - Provides an analytic expression of $\mathbf{A}$ on planes of constant $z$ → Symplectic tracking is possible
  - The equation $\nabla \cdot \mathbf{B} = 0$, while $\nabla \times \mathbf{B} = 0$ to a high order in the particle coordinates on planes of constant $z$.
- The representation can be computed from measured or simulated magnetic field data on a boundary
  - Orthogonal functions define the solution bases for circular, elliptical, and rectangular cylinders
  - Solutions typically converge quite rapidly
  - Fitting from boundary values tends to smooth any noise/errors in the data: difference between the ‘real’ and ‘generalized gradient’ field is a harmonic function whose maximum is on the boundary

[6] M. Venturini and A. Dragt. “Accurate computation of transfer maps from magnetic field data,” Nucl. Instrum. Methods Res. A **427**, 387 (1999).
[7] A. J. Dragt. *Lie Methods for Nonlinear Dynamics with Applications to Accelerator Physics*. Univ. of Maryland, College Park, 2020.
[8] C. E. Mitchell. “Calculation of Realistic charged-particle transfer maps.” PhD thesis, University of Maryland, College Park (2007).

# Tracking was added to `elegant`[9] using the `BGGEXP` element

- `BGGEXP` integrates particles through a field described by generalized gradients
  - Symplectic integrator using implicit midpoint method
    - Evaluates the vector potential $\boldsymbol{A}$ and updates the coordinates to locations between the data
    - Requires iteration for convergence
  - Nonsymplectic predictor-corrector
    - Explicit, only needs $B$-field components → over 3 times faster
- Tracking through quadrupoles, sextupoles, wigglers, etc. is relatively straightforward

[9] M. Borland, "elegant: A Flexible SDDS-Compliant Code for Accelerator Simulation", LS-287 (2000).
[10] D. Sagan, E. Hamwi, and P Nishikawa. "Generalized Gradient field description using the Bmad and PRC Toolkits," IPAC23, WEPL015 (2023), pp. 3136.
[11] W. Lin, D. Sagan, E. Hamwi, G. Hoffstaetter, and V. Schoefer, "Generalized gradient tracking in the Siberian snakes of the AGS and RHIC," IPAC23, WEPA064 (2023), pp. 2793

# Tracking was added to `elegant`[9] using the `BGGEXP` element

- `BGGEXP` integrates particles through a field described by generalized gradients
  - Symplectic integrator using implicit midpoint method
    - Evaluates the vector potential $A$ and updates the coordinates to locations between the data
    - Requires iteration for convergence
  - Nonsymplectic predictor-corrector
    - Explicit, only needs $B$-field components → over 3 times faster
- Tracking through quadrupoles, sextupoles, wigglers, etc. is relatively straightforward
- Tracking through dipoles requires also defining input and out planes, and using field scaling parameters to ensure correct bending angle
- Tracking through gradient dipoles requires careful setup
  - Small changes in initial $x$ will change the integrated bending field
  - Fine-tuning of the strength and/or $x$-offset is typically needed
- Similar capabilities have been added to Bmad[10,11]

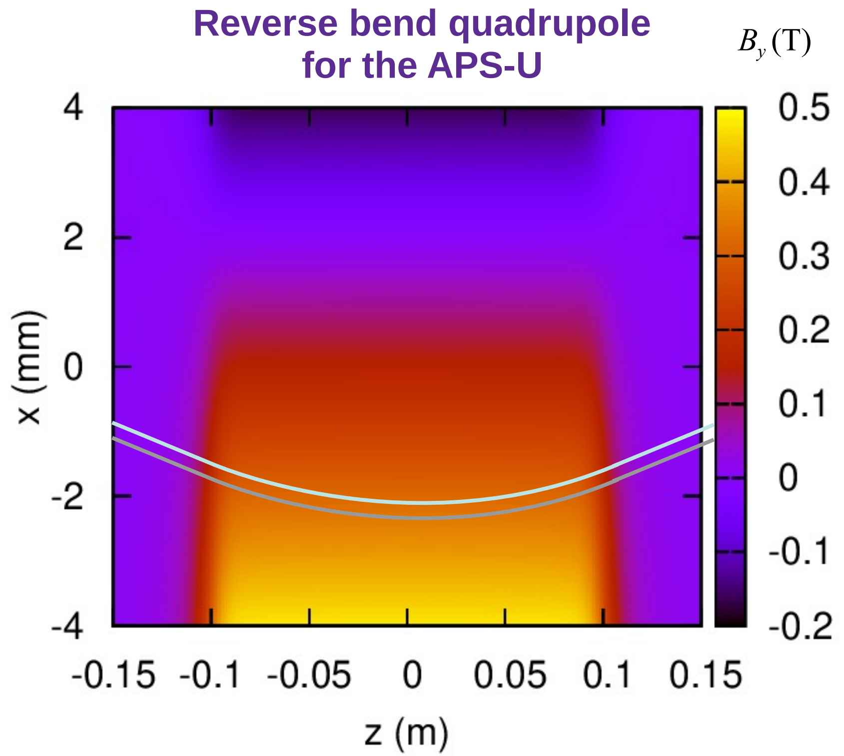



[9] M. Borland, “elegant: A Flexible SDDS-Compliant Code for Accelerator Simulation”, LS-287 (2000).
[10] D. Sagan, E. Hamwi, and P Nishikawa. “Generalized Gradient field description using the Bmad and PRC Toolkits,” IPAC23, WEPL015 (2023), pp. 3136.
[11] W. Lin, D. Sagan, E. Hamwi, G. Hoffstaetter, and V. Schoefer, “Generalized gradient tracking in the Siberian snakes of the AGS and RHIC,” IPAC23, WEPA064 (2023), pp. 2793

# Companion programs[12] use field data to compute the generalized gradient expansion for `elegant` tracking

- `computeCBGGE` uses the field data on the surface of a circular cylinder using equations from[6]
- `computeRBGGE` uses the field data on the surface of a rectangular cylinder using equations from[8]

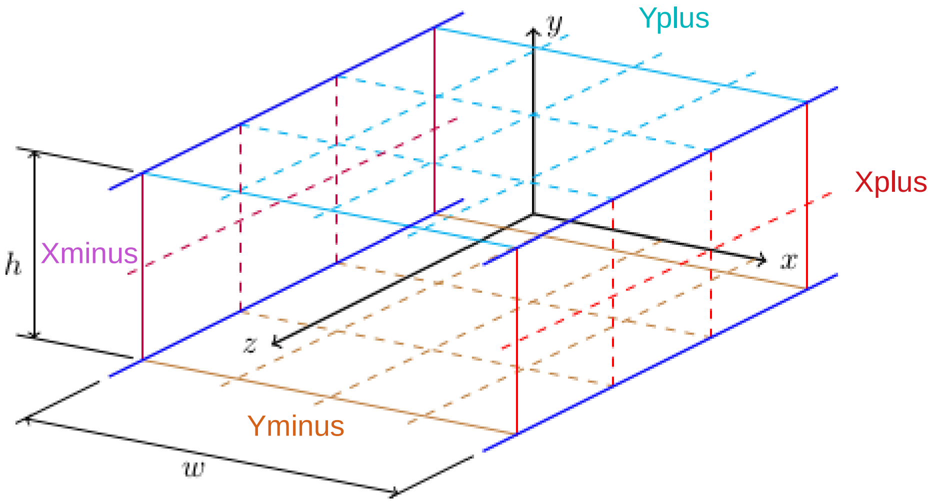


Normal field components on a rectangular cylinder define inputs for `computeRBGGE`


[12] M. Borland, R. R. Lindberg, R. Soliday, and A. Xiao, "Tools for Use of Generalized Gradient Expansions in Accelerator Simulations," in Proc. IPAC'21, pp. 253
[6] M. Venturini and A. Dragt. "Accurate computation of transfer maps from magnetic field data," Nucl. Instrum. Methods Res. A **427**, 387 (1999).
[8] C. E. Mitchell. "Calculation of Realistic charged-particle transfer maps." PhD thesis, University of Maryland, College Park (2007).

# Companion programs[12] use field data to compute the generalized gradient expansion for `elegant` tracking

- `computeCBGGE` uses the field data on the surface of a circular cylinder using equations from[6]
- `computeRBGGE` uses the field data on the surface of a rectangular cylinder using equations from[8]
- Both programs have several common features
  1. Choice of computing the normal, skew, or both field components
  2. Automated routine that finds the number of multipoles and derivatives to best match data
  3. Parallel computing using OpenMP
  4. Output files in a format suitable for the `BGGEXP` tracking element in `elegant`[9]

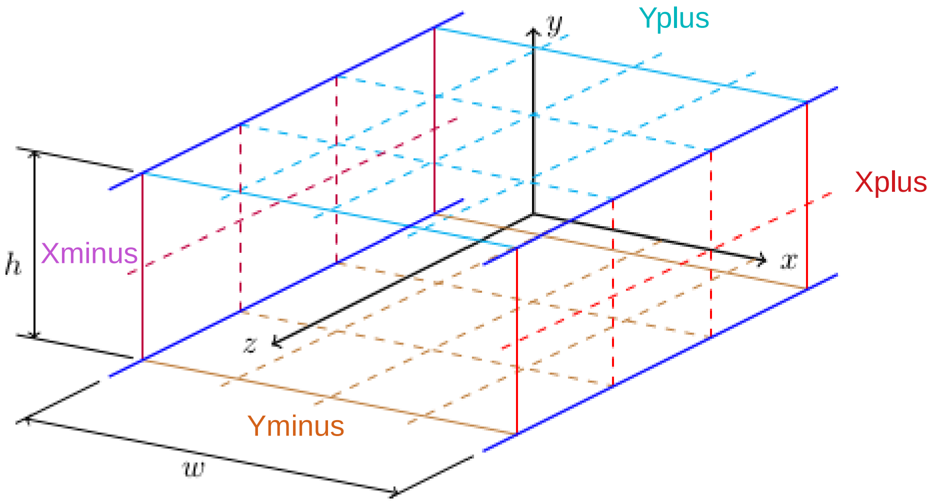


Normal field components on a rectangular cylinder define inputs for `computeRBGGE`


[12] M. Borland, R. R. Lindberg, R. Soliday, and A. Xiao, "Tools for Use of Generalized Gradient Expansions in Accelerator Simulations," in Proc. IPAC'21, pp. 253
[6] M. Venturini and A. Dragt. "Accurate computation of transfer maps from magnetic field data," Nucl. Instrum. Methods Res. A **427**, 387 (1999).
[8] C. E. Mitchell. "Calculation of Realistic charged-particle transfer maps." PhD thesis, University of Maryland, College Park (2007).
[9] M. Borland, "elegant: A Flexible SDDS-Compliant Code for Accelerator Simulation", LS-287 (2000).

# Application to APS-U's hybrid 7⁺BA lattice[13]; $\varepsilon_x$ = 42 pm[14]

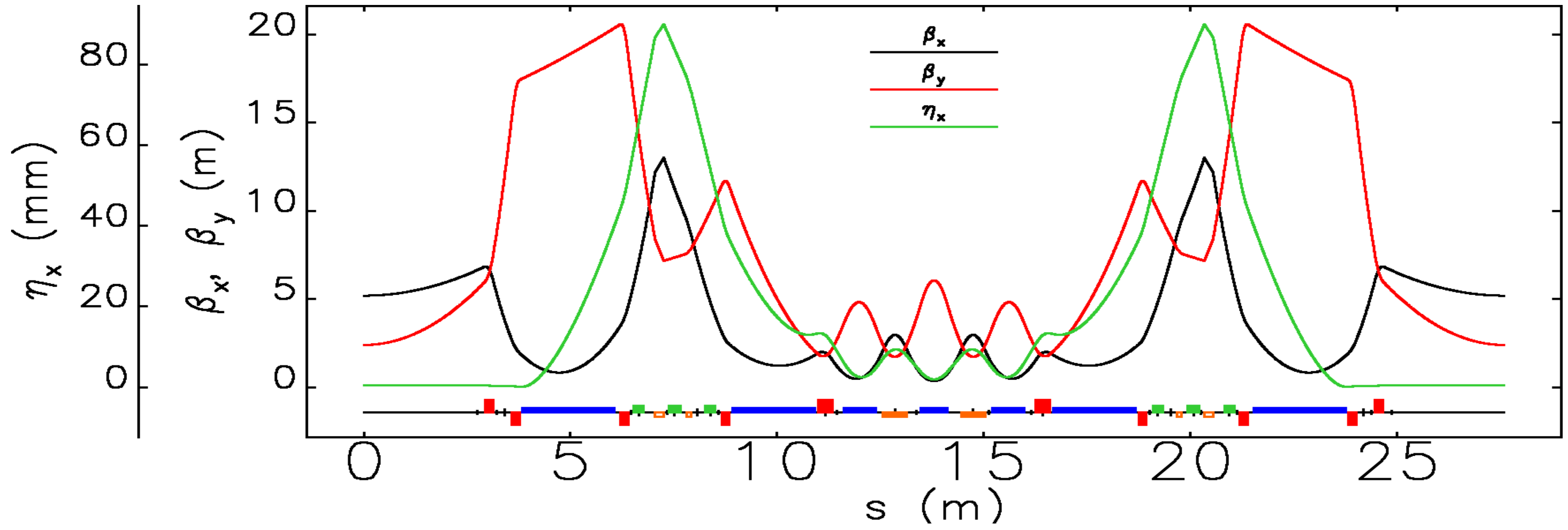


Dipoles

Reverse bend dipoles

Quadrupoles

Sextupoles


[13] L. Farvacque *et al.* "A Low-Emittance Lattice for the ESRF," IPAC 2013, pp 79; L. Farvacque, *et al.,* "ESRF-EBS Design Report," ed. by D. Einfeld and P. Raimondi (2018).

[14] M. Borland, Y. Sun, V. Sajaev, R. R. Lindberg, and T. Berenc. "Lower Emittance Lattice for the Advanced Photon Source Upgrade Using Reverse Bending Magnets," in NAPAC 2016, pp. 877

# Application to APS-U's hybrid 7+BA lattice[13]; $\varepsilon_x$ = 42 pm[14]

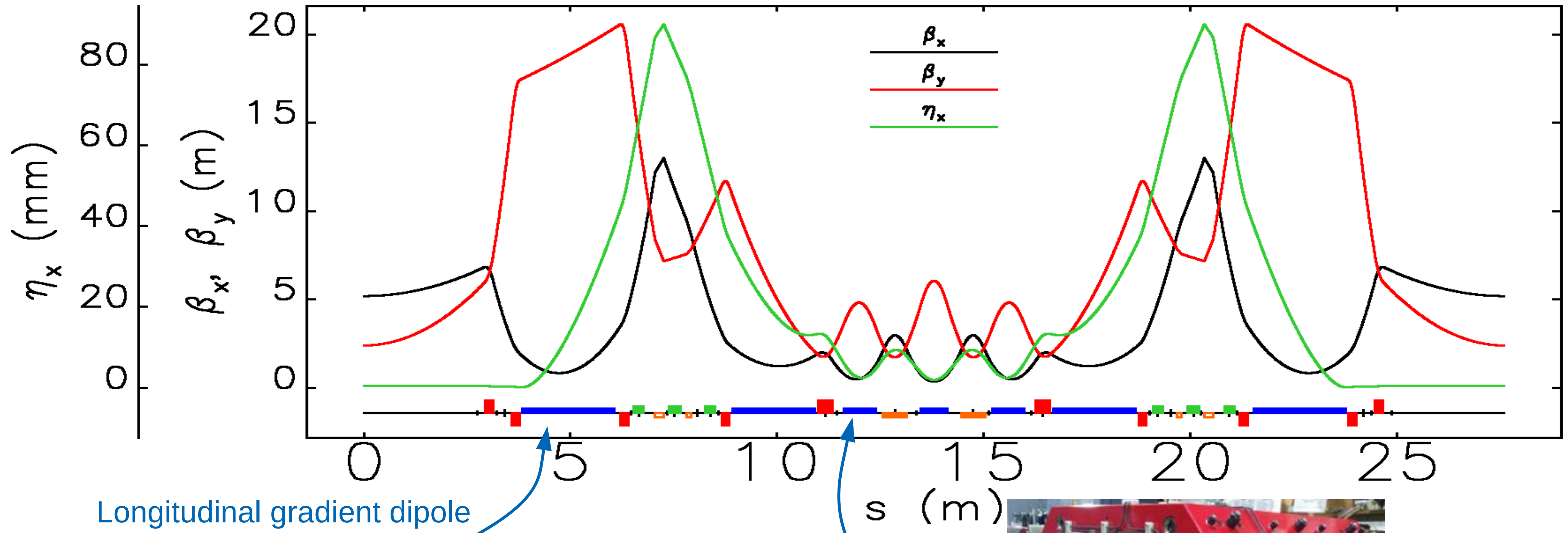


Dipoles

Reverse bend dipoles

Quadrupoles

Sextupoles

Longitudinal gradient dipole

Transverse gradient dipole

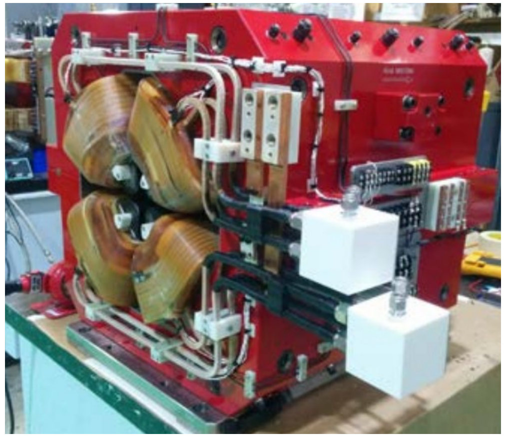

[13] L. Farvacque *et al.* "A Low-Emittance Lattice for the ESRF," IPAC 2013, pp 79; L. Farvacque, *et al.,* "ESRF-EBS Design Report," ed. by D. Einfeld and P. Raimondi (2018).
[14] M. Borland, Y. Sun, V. Sajaev, R. R. Lindberg, and T. Berenc. "Lower Emittance Lattice for the Advanced Photon Source Upgrade Using Reverse Bending Magnets," in NAPAC 2016, pp. 877

# Application to APS-U's hybrid 7⁺BA lattice[13]; $\varepsilon_x$ = 42 pm[14]

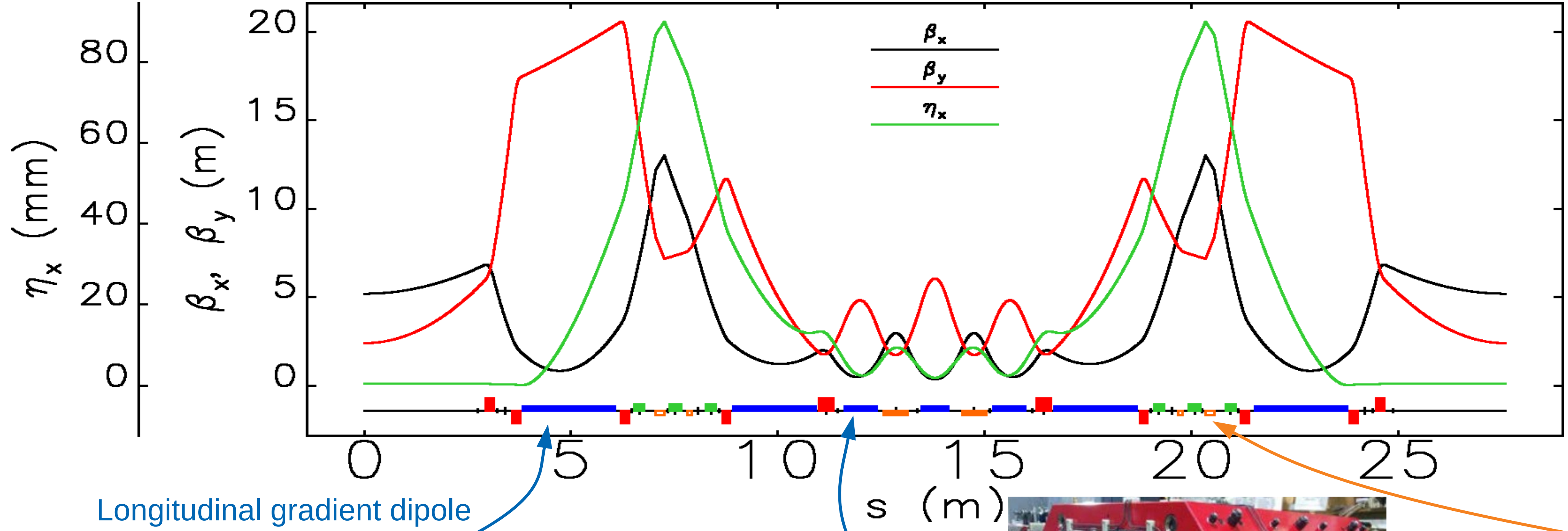


Dipoles

Reverse bend dipoles

Quadrupoles

Sextupoles

Longitudinal gradient dipole

Transverse gradient dipole

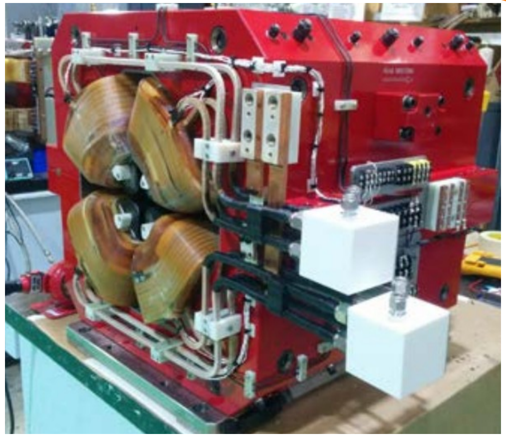

Transverse gradient reverse bend


[13] L. Farvacque *et al.* "A Low-Emittance Lattice for the ESRF," IPAC 2013, pp 79; L. Farvacque, *et al.,* "ESRF-EBS Design Report," ed. by D. Einfeld and P. Raimondi (2018).
[14] M. Borland, Y. Sun, V. Sajaev, R. R. Lindberg, and T. Berenc. "Lower Emittance Lattice for the Advanced Photon Source Upgrade Using Reverse Bending Magnets," in NAPAC 2016, pp. 877

# Generalized gradients from simulated magnetic data

$x$-$z$ cut of $B_y$ (T) from `OPERA` of the APS-U's Q4 reverse bend transverse gradient dipole[15]

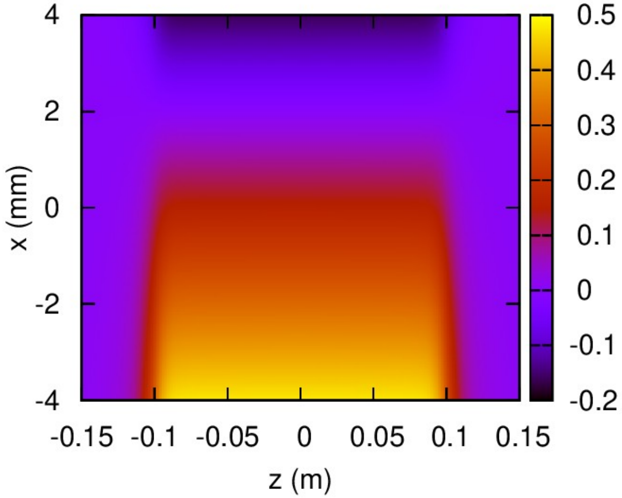


1. Start with simulation data

[15] M. Jaski et al. "Magnet Designs for the Multi-bend Achromat Lattice at the Advanced Photon Source," in Proc. IPAC'15, pp. 3260.

# Generalized gradients from simulated magnetic data

$x$-$z$ cut of $B_y$ (T) from `OPERA` of the APS-U's Q4 reverse bend transverse gradient dipole[15]

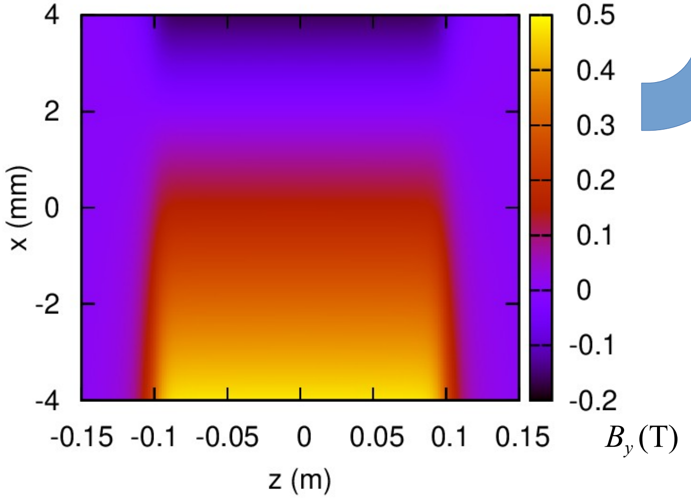


$\boldsymbol{B} \cdot \boldsymbol{n}$ on 10 mm radius cylinder

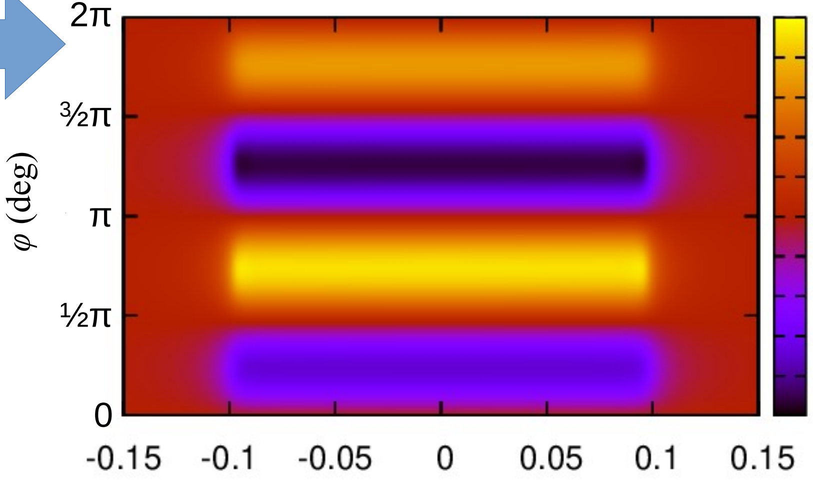


1. Start with simulation data
2. Evaluate normal component of **B** on a bounding surface

[15] M. Jaski et al. "Magnet Designs for the Multi-bend Achromat Lattice at the Advanced Photon Source," in Proc. IPAC'15, pp. 3260.

# Generalized gradients from simulated magnetic data

$x$-$z$ cut of $B_y$ (T) from `OPERA` of the APS-U's Q4 reverse bend transverse gradient dipole[15]

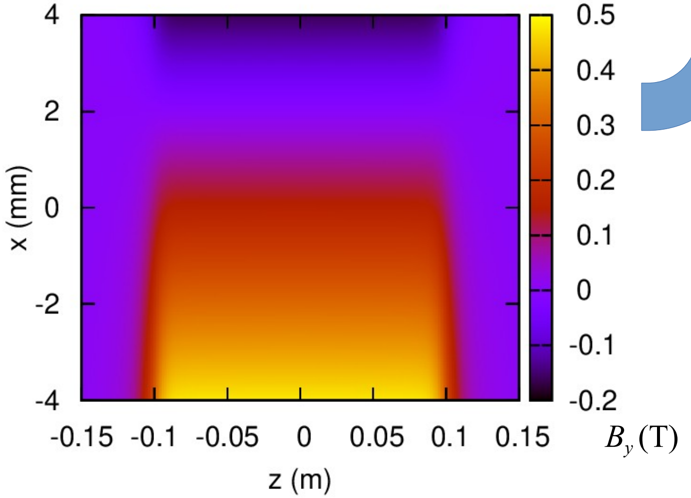


$\boldsymbol{B} \cdot \boldsymbol{n}$ on 10 mm radius cylinder

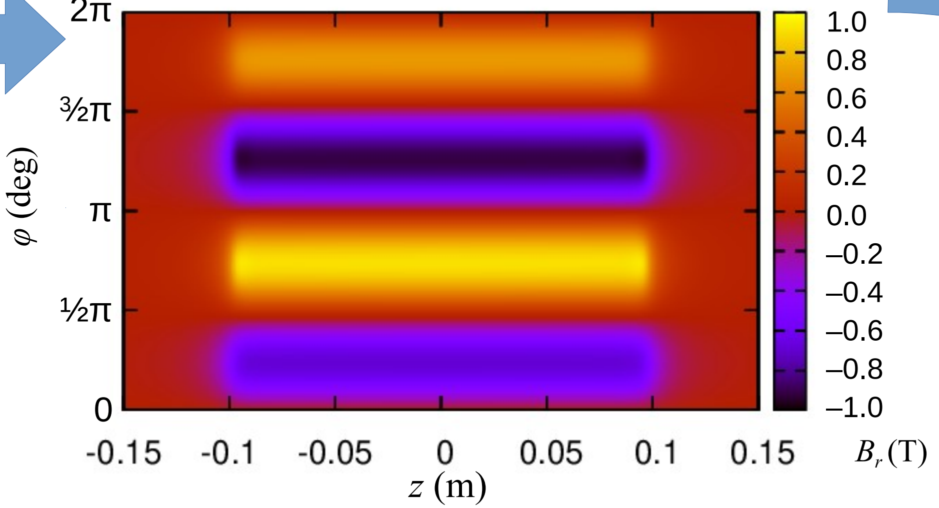


Use `computeCBGGE` to compute generalized gradients

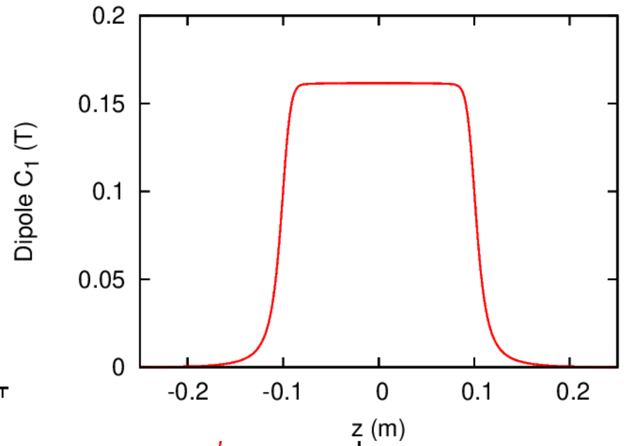


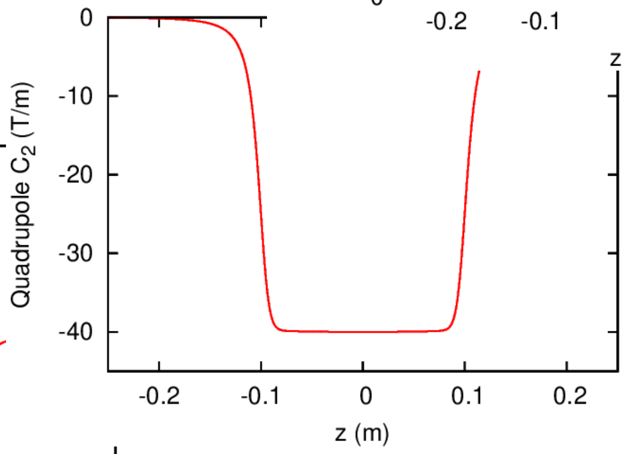


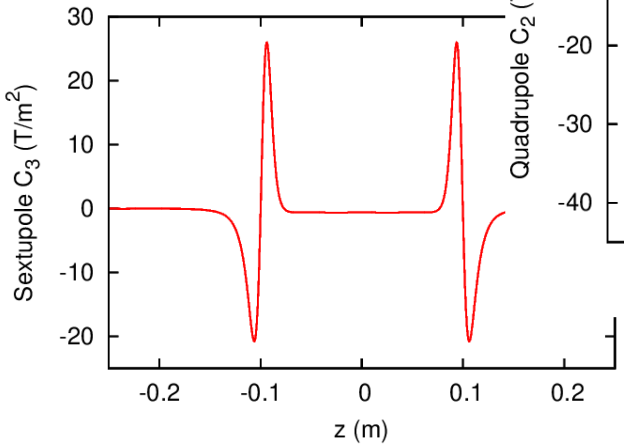


1. Start with simulation data
2. Evaluate normal component of **B** on a bounding surface
3. Compute and retain generalized gradients that minimize $\Delta\mathbf{B}$ on the boundary

+ higher order multipoles
+ their $z$ derivatives


[15] M. Jaski et al. "Magnet Designs for the Multi-bend Achromat Lattice at the Advanced Photon Source," in Proc. IPAC'15, pp. 3260.

# Generalized gradients from simulated magnetic data

*x-z* cut of $B_y$ (T) from `OPERA` of the APS-U's Q4 reverse bend transverse gradient dipole[15]

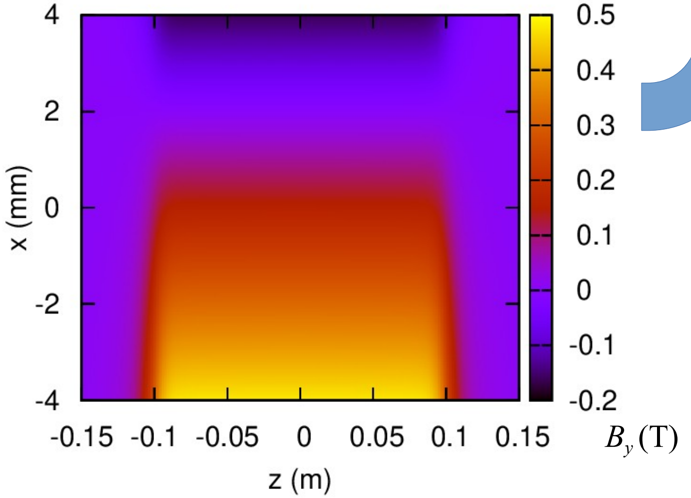


$\boldsymbol{B} \cdot \boldsymbol{n}$ on 10 mm radius cylinder

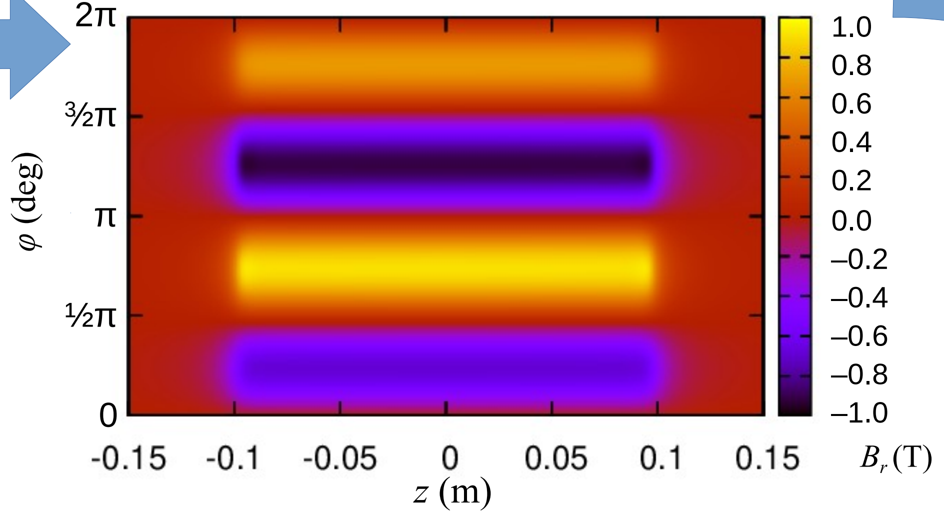


Use `computeCBGGE` to compute generalized gradients

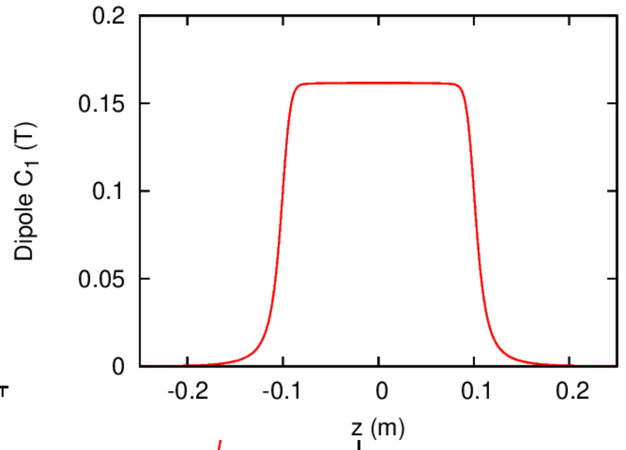


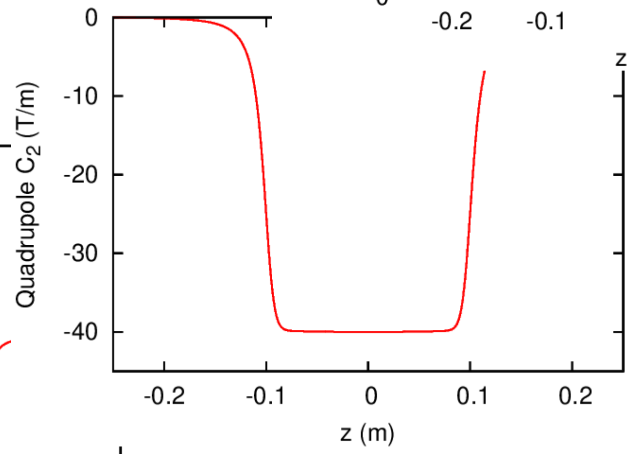


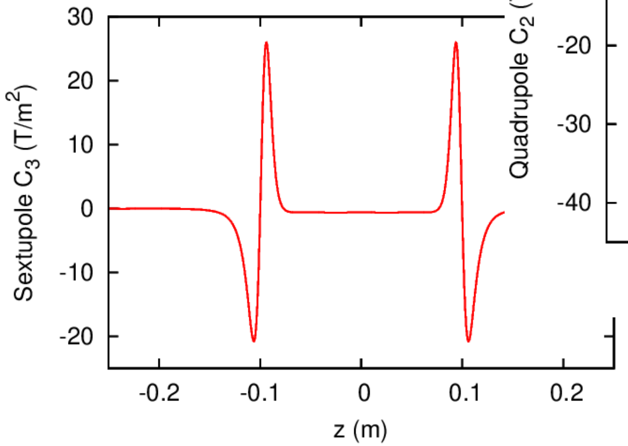


+ higher order multipoles
+ their *z* derivatives

1. Start with simulation data
2. Evaluate normal component of **B** on a bounding surface
3. Compute and retain generalized gradients that minimize $\Delta\mathbf{B}$ on the boundary
4. Use in tracking


[15] M. Jaski et al. "Magnet Designs for the Multi-bend Achromat Lattice at the Advanced Photon Source," in Proc. IPAC'15, pp. 3260.

# Model of the longitudinal gradient dipole looks good

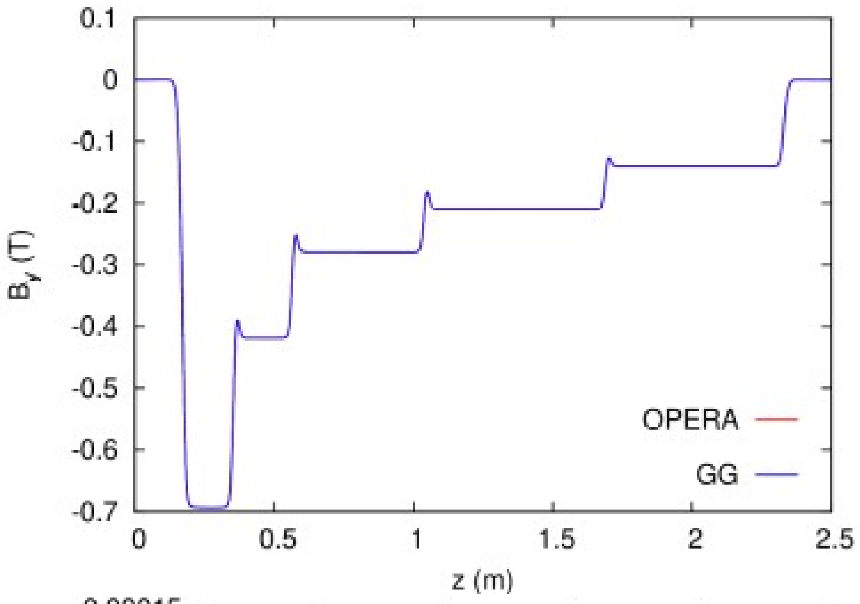


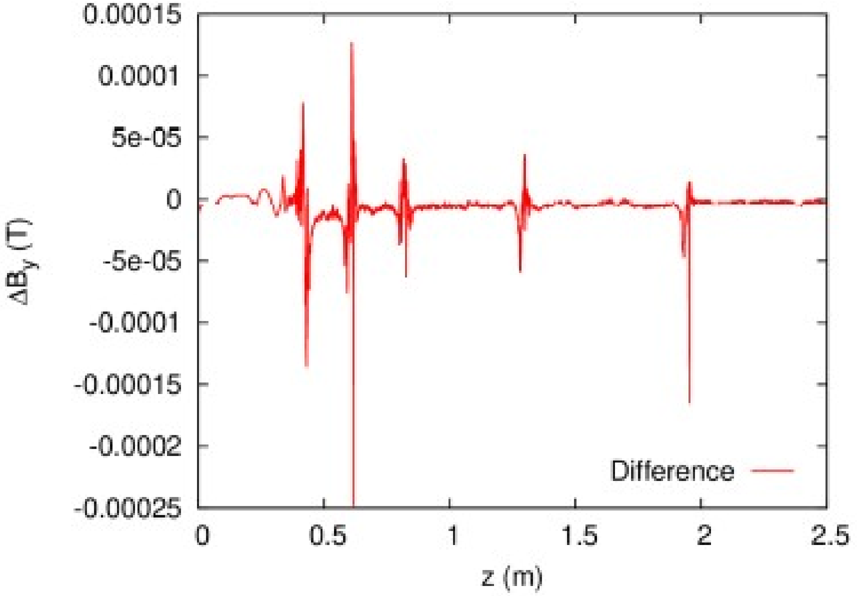

# Model of the longitudinal gradient dipole looks good

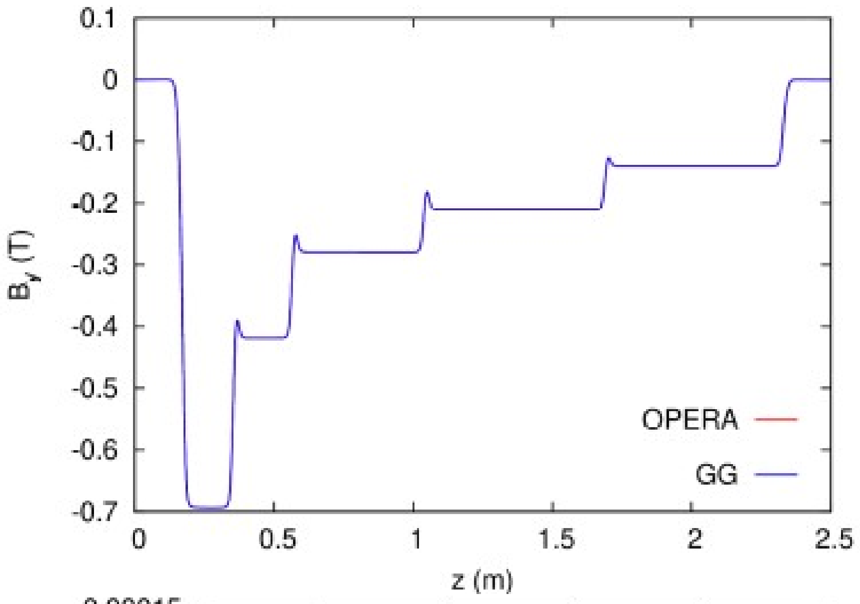


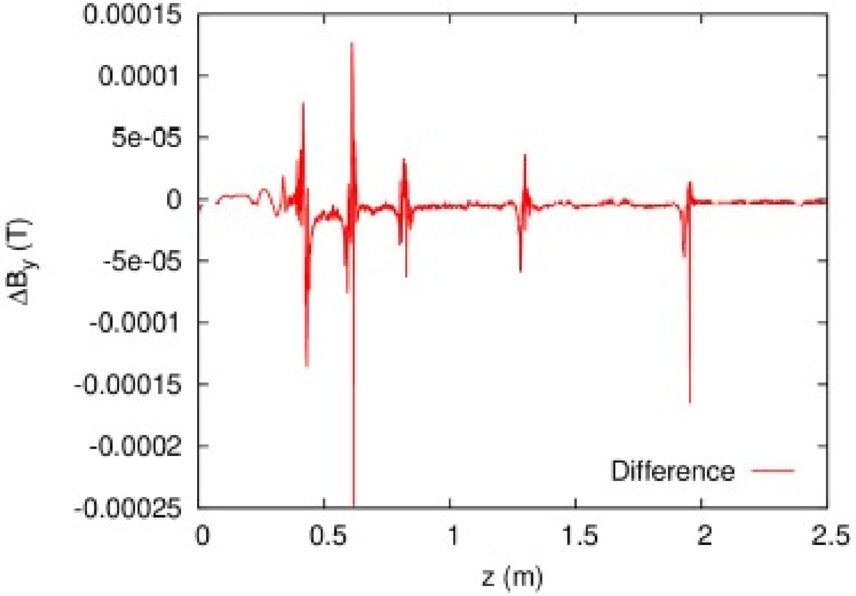


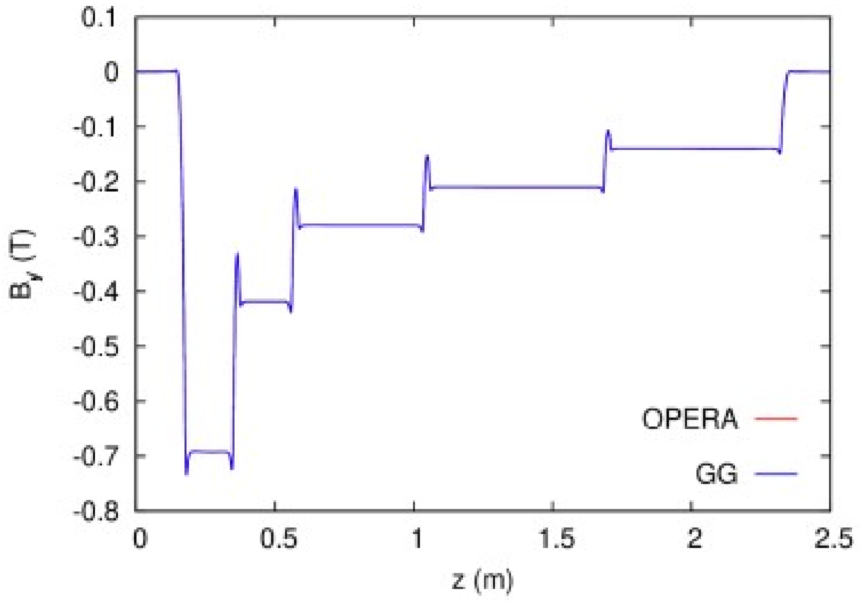


**Comparison at the top of the box**

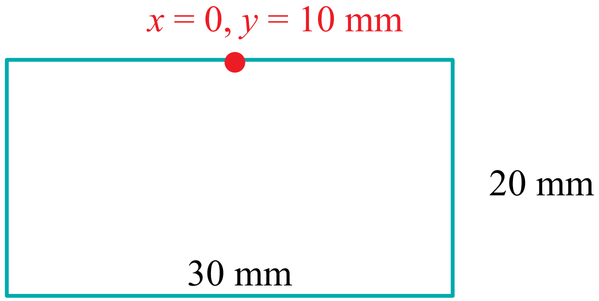


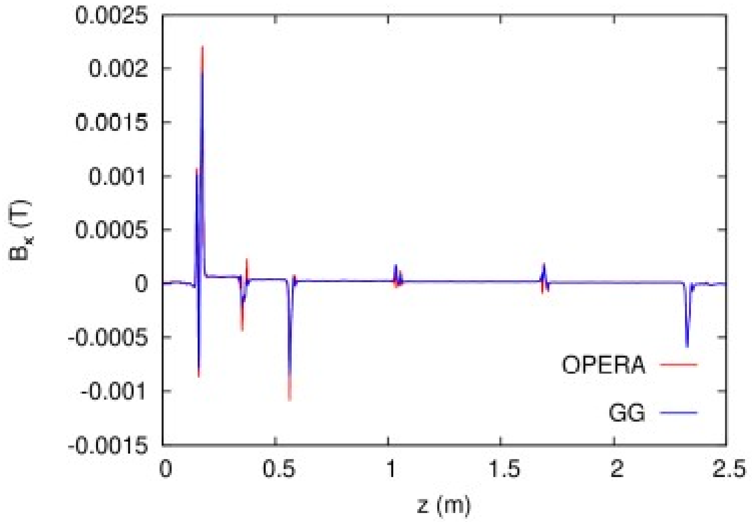


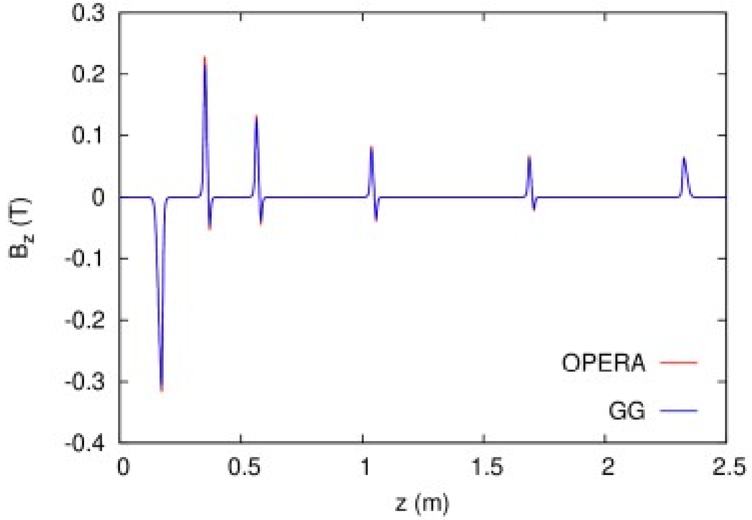

# All-GGE lattice of APS-U tuned to match design[16]

- We used `OPERA` data from M. Jaski to assemble an all-GGE APS-U lattice model
- Matching of models requires two steps
  - Tune each GGE element to match the 2nd order properties of each magnet
  - Apply global tuning to control the orbit and reproduce the linear optics and chromaticity

[16] R.Lindberg and M. Borland. “Storage ring tracking using generalized gradient representation of full magnetic field maps,” in Proc. of the 2022 NAPAC, pp. 542.

# All-GGE lattice of APS-U tuned to match design[16]

- We used OPERA data from M. Jaski to assemble an all-GGE APS-U lattice model
- Matching of models requires two steps
  - Tune each GGE element to match the 2nd order properties of each magnet
  - Apply global tuning to control the orbit and reproduce the linear optics and chromaticity
- This is laborious, but works well
  - Relies on the numerical computation of 2nd-order transport matrices[17]
  - Optimization is only practical because of parallelization[18]

APS-U lattice from hard edge models: black

APS-U lattice using GGEs for each magnet: red

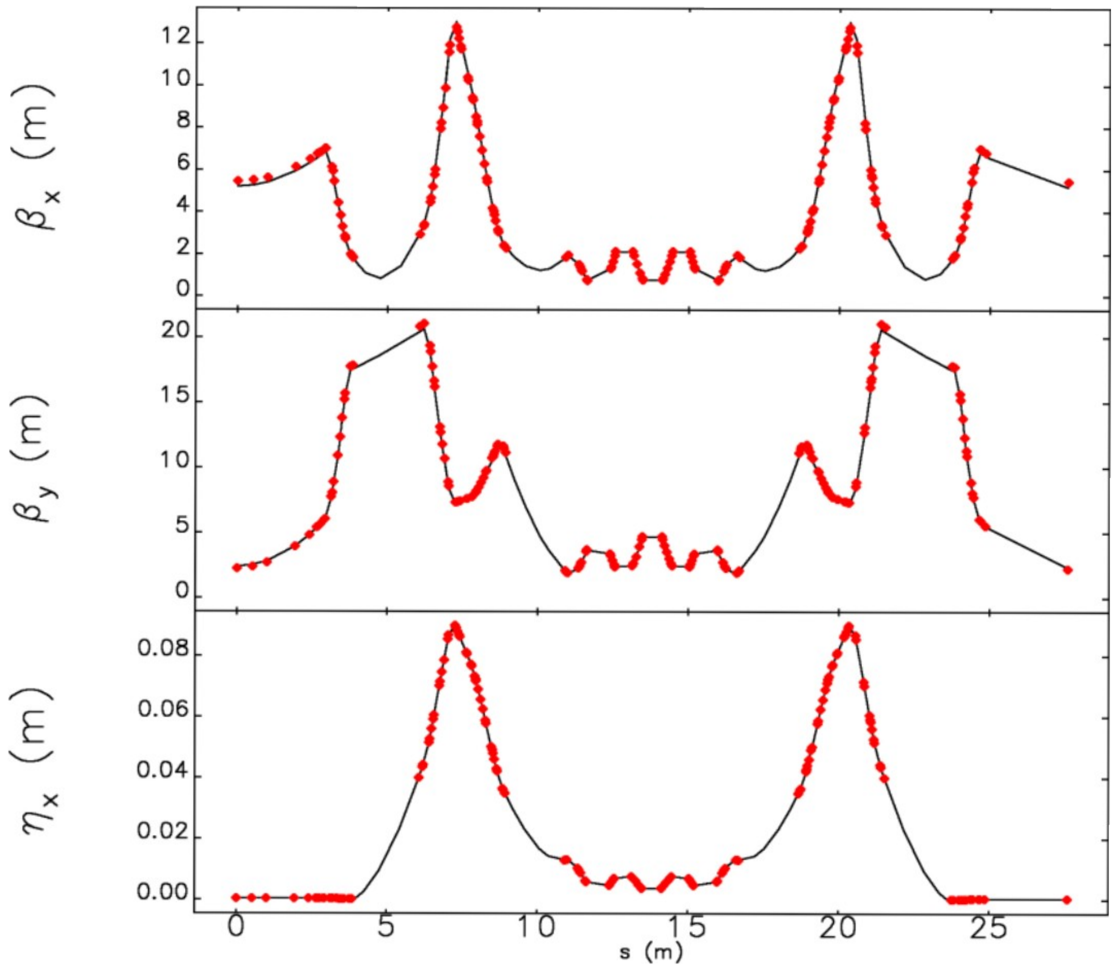



[16] R.Lindberg and M. Borland. “Storage ring tracking using generalized gradient representation of full magnetic field maps,” in Proc. of the 2022 NAPAC, pp. 542.

[17] M. Borland, “A High-Brightness thermionic microwave electron gun,” PhD thesis, Stanford University, SLAC-402, (1991).

[18] Y. Wang and M. Borland, “Pelegant: A Parallel Accelerator Simulation Code for Electron Generation and Tracking,” AIP Conf. Proc., 877, 241 (2006).

# Chromatic tune footprint matches fairly well

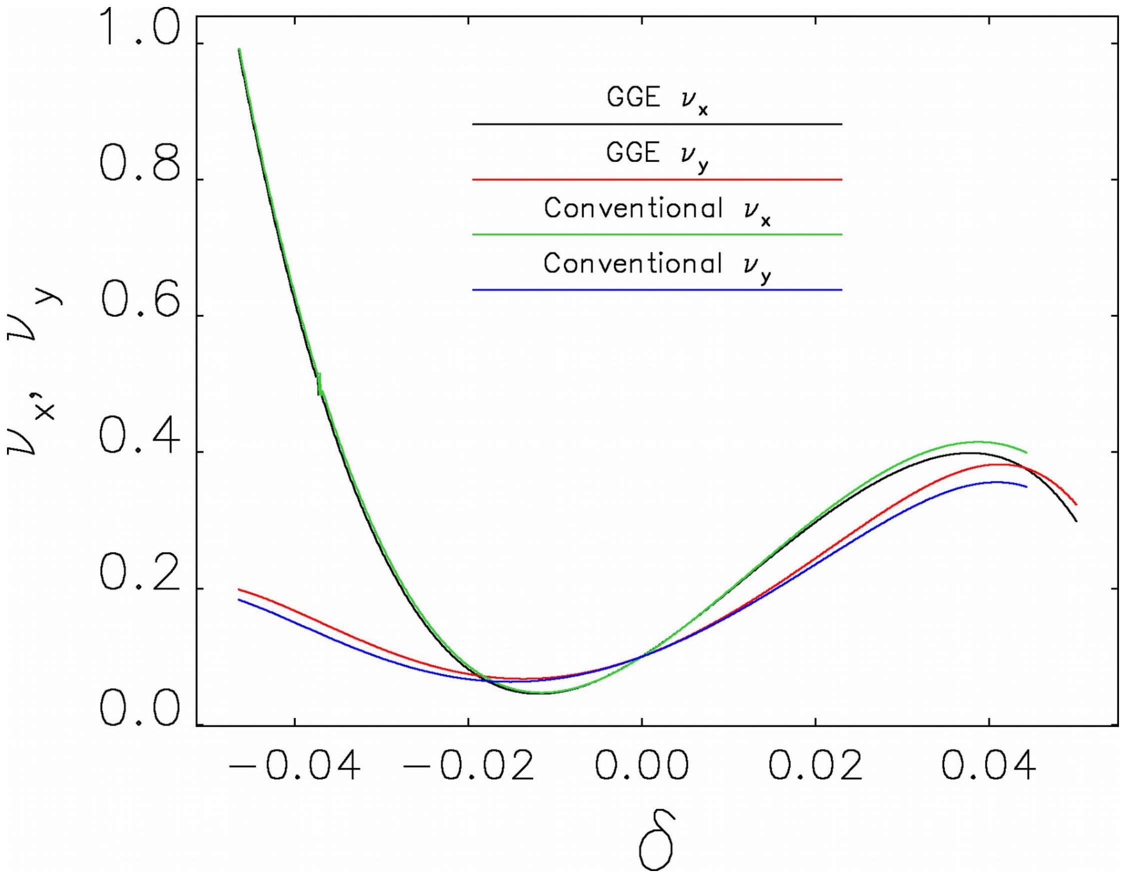


- The tune's dependence on energy is quite close over the entire range
- GGE "tuning" only matched linear optics and chromaticities
- GGE tracking takes about 280 times longer

# Chromatic tune footprint matches fairly well

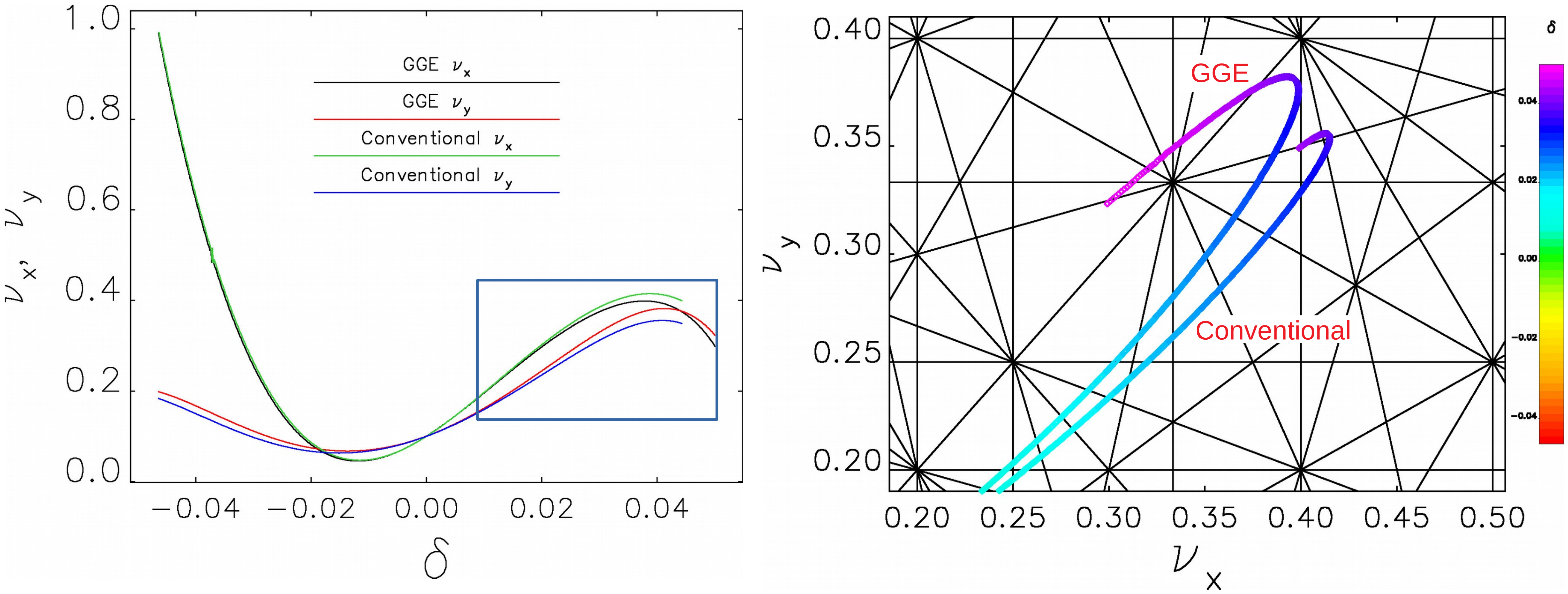


- The tune's dependence on energy is quite close over the entire range
- GGE "tuning" only matched linear optics and chromaticities
- GGE tracking takes about 280 times longer

# Nonlinear dynamics are similar

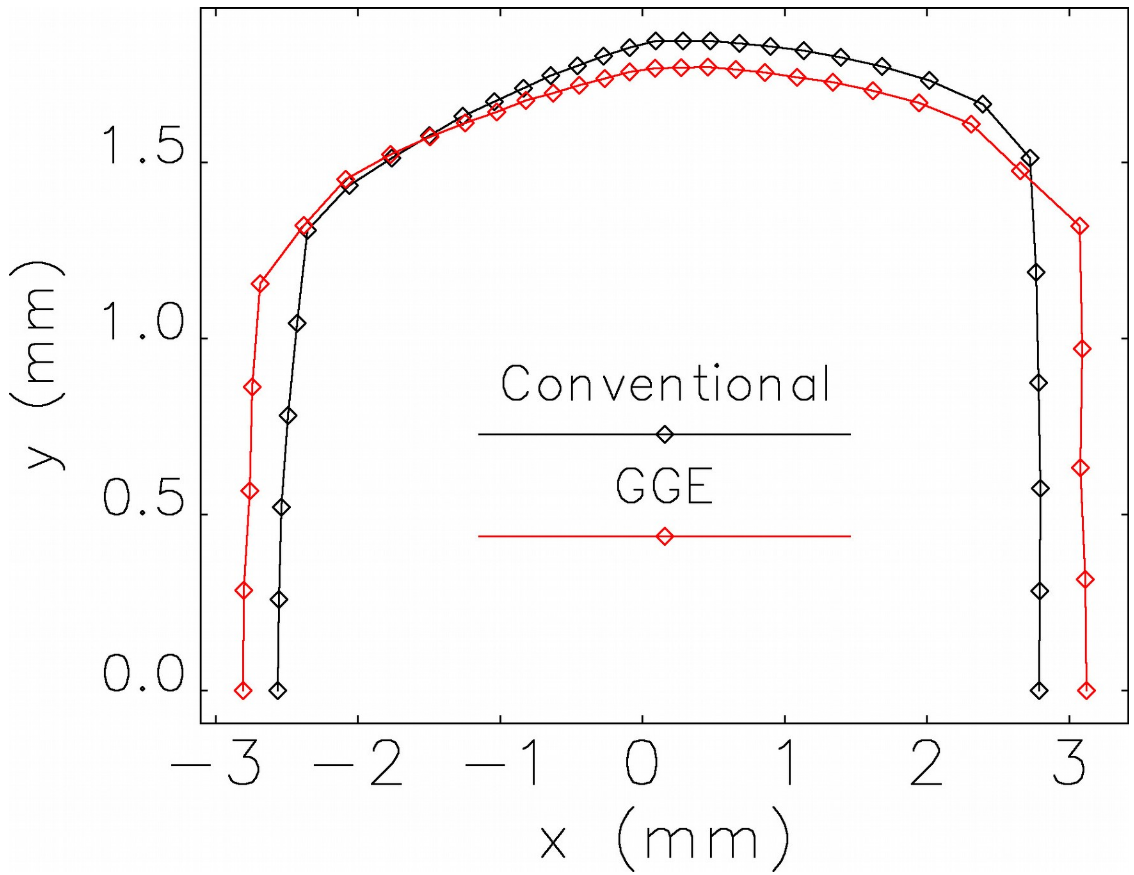


- The predictions for the dynamic acceptance agree reasonably well

# Nonlinear dynamics are similar

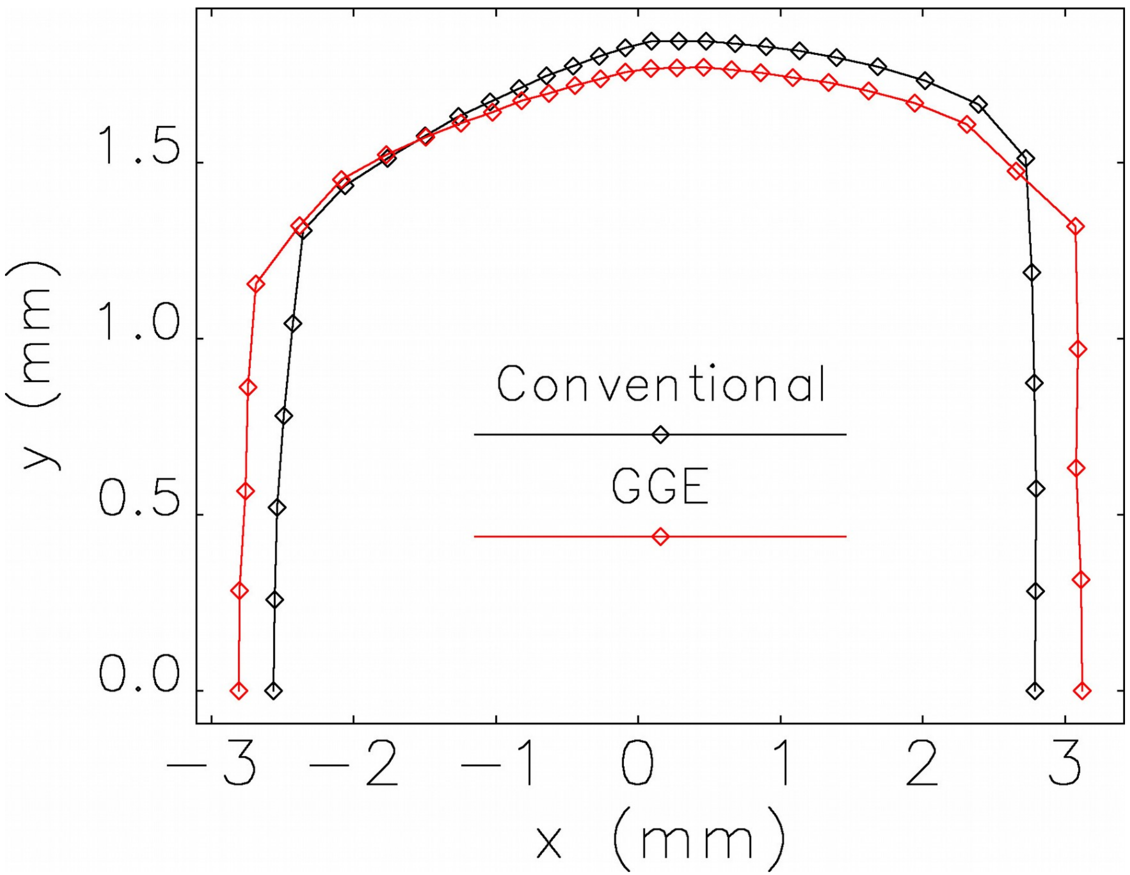


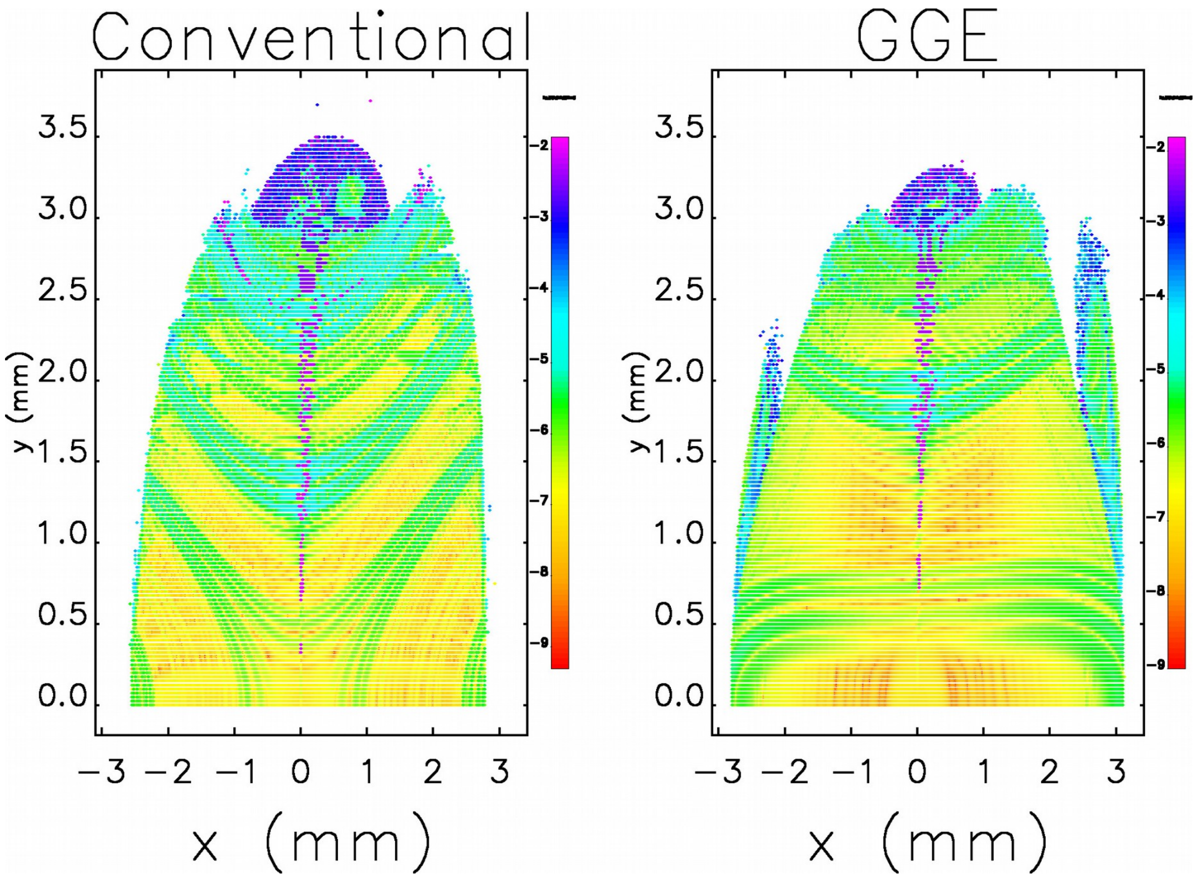


- The predictions for the dynamic acceptance agree reasonably well
- The frequency maps are vaguely similar
  - Same overall shape, but clearly different details
  - We are investigating possible sources of discrepancy

# The magnitude of the GGE tuning indicates that some hard-edge models could be improved

- After tuning the GGE model, the straight magnets have integrated strengths very close to design values

Comparison of integrated strength

| Magnet Name | Design to GGE ratio | Design length (m) | GGE length (m) |
|---|---|---|---|
| Q1 | 1.0107 | 0.20495 | 0.20492 |
| Q2 | 1.0002 | 0.17918 | 0.17916 |
| Q3 | 0.9979 | 0.18009 | 0.18005 |
| Q6 | 1.0010 | 0.18010 | 0.17974 |
| Q7 | 0.9967 | 0.35655 | 0.35655 |
| S01A:S1 | 0.9924 | 0.18050 | 0.18046 |
| S01A:S2 | 0.9892 | 0.21075 | 0.21056 |
| S01A:S3 | 0.9924 | 0.18050 | 0.18046 |
| S01B:S1 | 0.9924 | 0.18050 | 0.18046 |
| S01B:S2 | 0.9892 | 0.21075 | 0.21056 |
| S01B:S3 | 0.9924 | 0.18050 | 0.18046 |
| S02A:S1 | 0.9924 | 0.18050 | 0.18046 |
| S02A:S2 | 0.9892 | 0.21075 | 0.21056 |
| S02A:S3 | 0.9924 | 0.18050 | 0.18046 |
| S02B:S1 | 0.9924 | 0.18050 | 0.18046 |
| S02B:S2 | 0.9892 | 0.21075 | 0.21056 |
| S02B:S3 | 0.9924 | 0.18050 | 0.18046 |

# The magnitude of the GGE tuning indicates that some hard-edge models could be improved

- After tuning the GGE model, the straight magnets have integrated strengths very close to design values
- Matching the transverse gradient dipoles require changing the GGE dipole and quadrupole strengths by a few percent

Comparison of integrated strength

| Magnet Name | Design to GGE ratio | Design length (m) | GGE length (m) |
|---|---|---|---|
| Q1 | 1.0107 | 0.20495 | 0.20492 |
| Q2 | 1.0002 | 0.17918 | 0.17916 |
| Q3 | 0.9979 | 0.18009 | 0.18005 |
| Q6 | 1.0010 | 0.18010 | 0.17974 |
| Q7 | 0.9967 | 0.35655 | 0.35655 |
| S01A:S1 | 0.9924 | 0.18050 | 0.18046 |
| S01A:S2 | 0.9892 | 0.21075 | 0.21056 |
| S01A:S3 | 0.9924 | 0.18050 | 0.18046 |
| S01B:S1 | 0.9924 | 0.18050 | 0.18046 |
| S01B:S2 | 0.9892 | 0.21075 | 0.21056 |
| S01B:S3 | 0.9924 | 0.18050 | 0.18046 |
| S02A:S1 | 0.9924 | 0.18050 | 0.18046 |
| S02A:S2 | 0.9892 | 0.21075 | 0.21056 |
| S02A:S3 | 0.9924 | 0.18050 | 0.18046 |
| S02B:S1 | 0.9924 | 0.18050 | 0.18046 |
| S02B:S2 | 0.9892 | 0.21075 | 0.21056 |
| S02B:S3 | 0.9924 | 0.18050 | 0.18046 |

Tuning parameters for transverse gradient dipoles

| Element Name | Dipole Factor | Quadrupole Factor | DX (mm) |
|---|---|---|---|
| Q4 | 1.0171 | 1.0028 | -0.024 |
| Q5 | 0.9681 | 0.9948 | 0.009 |
| M3 | 0.9842 | 1.0017 | 0.012 |
| Q8 | 1.0138 | 1.0118 | -0.021 |
| M4 | 0.9833 | 1.0117 | -0.077 |

# The magnitude of the GGE tuning indicates that some hard-edge models could be improved

- After tuning the GGE model, the straight magnets have integrated strengths very close to design values
- Matching the transverse gradient dipoles require changing the GGE dipole and quadrupole strengths by a few percent
- Matching the longitudinal gradient dipoles requires small strength adjustments, but large (~2 mm) longitudinal displacements.
  - Hard edge model of longitudinal gradient dipole has long been troublesome
  - Could we improve matters with better fringe field modeling?

Comparison of integrated strength

| Magnet Name | Design to GGE ratio | Design length (m) | GGE length (m) |
|---|---|---|---|
| Q1 | 1.0107 | 0.20495 | 0.20492 |
| Q2 | 1.0002 | 0.17918 | 0.17916 |
| Q3 | 0.9979 | 0.18009 | 0.18005 |
| Q6 | 1.0010 | 0.18010 | 0.17974 |
| Q7 | 0.9967 | 0.35655 | 0.35655 |
| S01A:S1 | 0.9924 | 0.18050 | 0.18046 |
| S01A:S2 | 0.9892 | 0.21075 | 0.21056 |
| S01A:S3 | 0.9924 | 0.18050 | 0.18046 |
| S01B:S1 | 0.9924 | 0.18050 | 0.18046 |
| S01B:S2 | 0.9892 | 0.21075 | 0.21056 |
| S01B:S3 | 0.9924 | 0.18050 | 0.18046 |
| S02A:S1 | 0.9924 | 0.18050 | 0.18046 |
| S02A:S2 | 0.9892 | 0.21075 | 0.21056 |
| S02A:S3 | 0.9924 | 0.18050 | 0.18046 |
| S02B:S1 | 0.9924 | 0.18050 | 0.18046 |
| S02B:S2 | 0.9892 | 0.21075 | 0.21056 |
| S02B:S3 | 0.9924 | 0.18050 | 0.18046 |

Tuning parameters for transverse gradient dipoles

| Element Name | Dipole Factor | Quadrupole Factor | DX (mm) |
|---|---|---|---|
| Q4 | 1.0171 | 1.0028 | -0.024 |
| Q5 | 0.9681 | 0.9948 | 0.009 |
| M3 | 0.9842 | 1.0017 | 0.012 |
| Q8 | 1.0138 | 1.0118 | -0.021 |
| M4 | 0.9833 | 1.0117 | -0.077 |

Tuning parameters for longitudinal gradient dipoles

| Element Name | Dipole Factor | DZ (mm) |
|---|---|---|
| AM1 | 0.9999 | -1.376 |
| AM2 | 0.9987 | 1.999 |
| BM2 | 0.9987 | -1.999 |
| BM1 | 0.9999 | 1.376 |

# Challenges for our choice of symplectic tracking

- The techniques described previously work well for magnets whose reference orbit is close to the $z$-axis (straight magnets and dipoles with small bending angles: APS-U dipoles have bending angle < 30 mrad)
- The representation of the magnetic field is less reliable for large bending angles (large sagitta)
  - Transverse Taylor series is about the $z$-axis, and may converge poorly at large $x$
  - Wide magnets with disparate length scales in $x$ and $y$ are particularly problematic

Dipole with 45 degree bend used in the APS Particle Accumulator Ring (PAR)

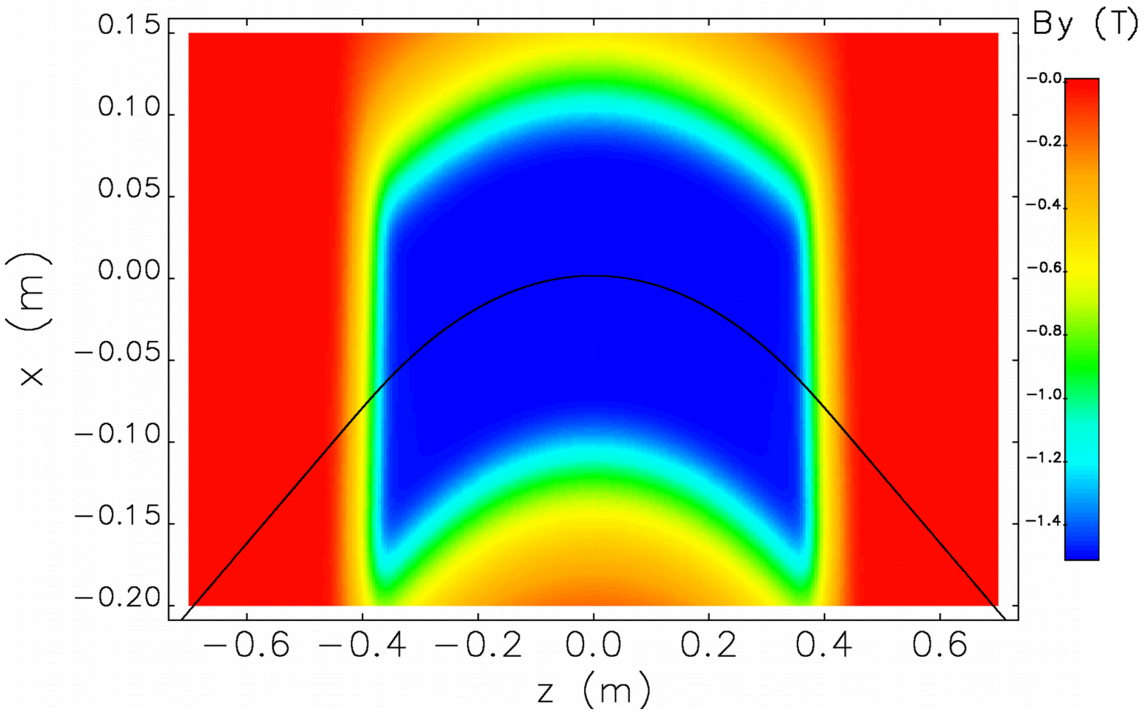

# Challenges for our choice of symplectic tracking

- The techniques described previously work well for magnets whose reference orbit is close to the $z$-axis (straight magnets and dipoles with small bending angles: APS-U dipoles have bending angle < 30 mrad)
- The representation of the magnetic field is less reliable for large bending angles (large sagitta)
  - Transverse Taylor series is about the $z$-axis, and may converge poorly at large $x$
  - Wide magnets with disparate length scales in $x$ and $y$ are particularly problematic
- As an extreme example, consider an infinitely wide whose magnetic potential $\psi = \sum_{p=0}^{\infty} \frac{(-1)^p y^{2p+1}}{(2p+1)!} C_1^{[2p]}(z)$
- We get this using our circular generalized gradient expansion if the coefficients satisfy

$$p \geq 1: \; C_{2p+1}(z) \rightarrow \frac{C_1^{[2p]}(z)}{4^p(2p+1)!}, \qquad C_{2p}(z) \rightarrow 0$$

- Hence, careful cancellation of high-order terms is required to properly model the dipole at large sagitta

Dipole with 45 degree bend used in the APS Particle Accumulator Ring (PAR)

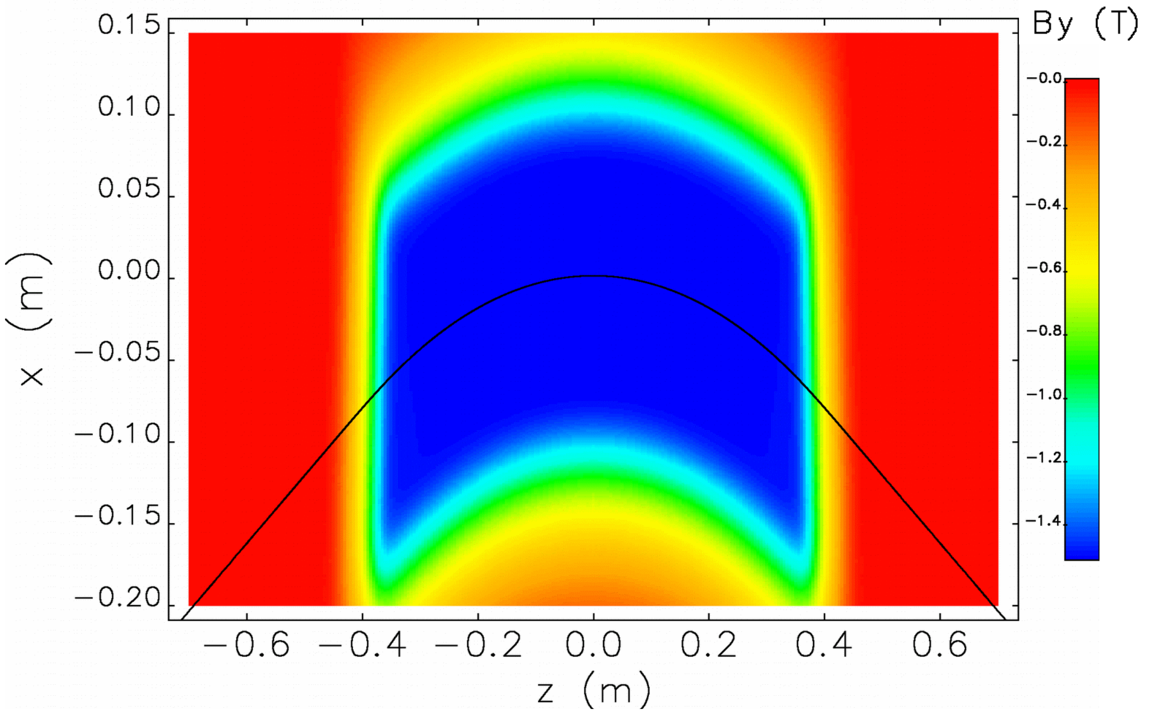

# Challenges for our choice of symplectic tracking

- The techniques described previously work well for magnets whose reference orbit is close to the z-axis (straight magnets and dipoles with small bending angles: APS-U dipoles have bending angle < 30 mrad)
- The representation of the magnetic field is less reliable for large bending angles (large sagitta)
  - Transverse Taylor series is about the $z$-axis, and may converge poorly at large $x$
  - Wide magnets with disparate length scales in $x$ and $y$ are particularly problematic
- As an extreme example, consider an infinitely wide whose magnetic potential $$\psi = \sum_{p=0}^{\infty} \frac{(-1)^p y^{2p+1}}{(2p+1)!} C_1^{[2p]}(z)$$
- We get this using our circular generalized gradient expansion if the coefficients satisfy

$$p \geq 1: \; C_{2p+1}(z) \rightarrow \frac{C_1^{[2p]}(z)}{4^p (2p+1)!}, \qquad C_{2p}(z) \rightarrow 0$$

- Hence, careful cancellation of high-order terms is required to properly model the dipole at large sagitta
  - Increased sensitivity to numerical errors
  - Similar "feed-down" effects can plague multipole error terms in straight-pole magnets

Gradient dipole with 10 degree bend planned for the ALS-U Accumulator ring[19]

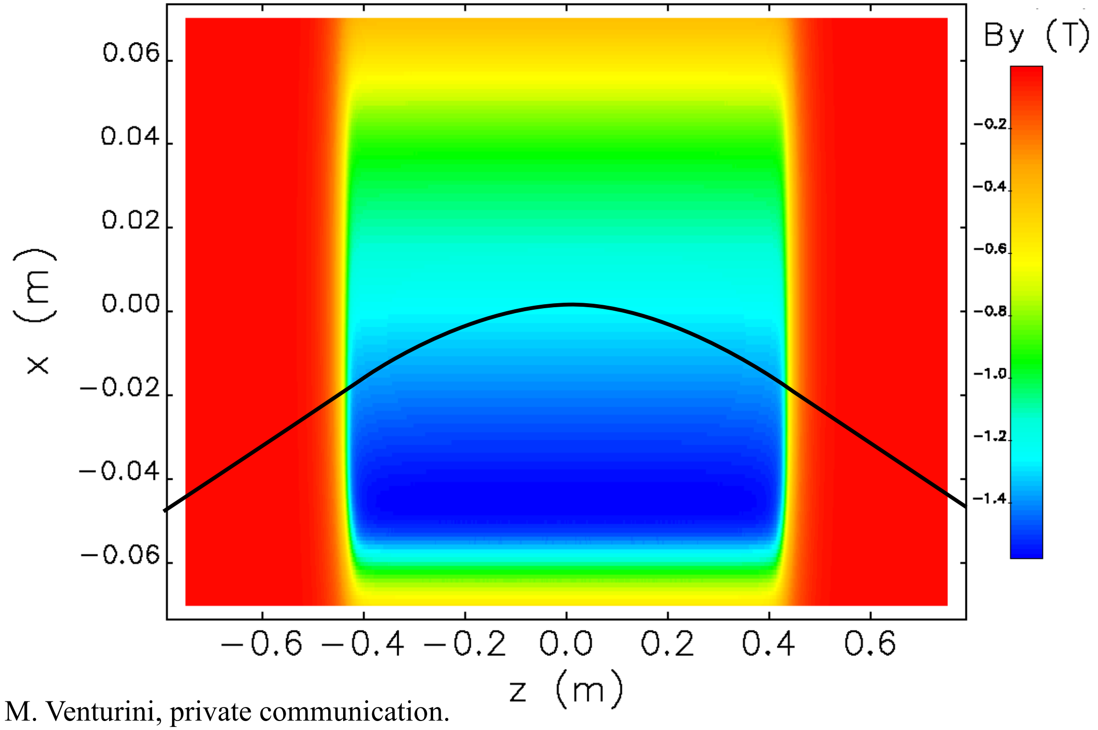


[19] M. Venturini, private communication.

# One fix is to expand field about reference orbit

- Boundary techniques of generalized gradients can be extended with "bent-box" method[8]

Normal component of B — Magnetic potential

$$\boldsymbol{A}(\boldsymbol{r}) = \int_{\partial V} dS' \;\left\{[\hat{\boldsymbol{n}}(\boldsymbol{r}')\cdot\boldsymbol{B}(\boldsymbol{r}')]\boldsymbol{G}^n[\boldsymbol{r}';\boldsymbol{r},\hat{\boldsymbol{m}}(\boldsymbol{r}')] + \psi(\boldsymbol{r}')\boldsymbol{G}^t[\boldsymbol{r};\boldsymbol{r}',\hat{\boldsymbol{n}}(\boldsymbol{r}')]\right\}$$

$$\frac{\boldsymbol{m}(\boldsymbol{r}')\times(\boldsymbol{r}-\boldsymbol{r}')}{4\pi\,|\boldsymbol{r}-\boldsymbol{r}'|-\hat{\boldsymbol{m}}(\boldsymbol{r}')\cdot(\boldsymbol{r}-\boldsymbol{r}')} \qquad \frac{\hat{\boldsymbol{n}}(\boldsymbol{r}')\times(\boldsymbol{r}-\boldsymbol{r}')}{4\pi\,|\boldsymbol{r}-\boldsymbol{r}'|^3}$$

  - First envisioned as employing a bounding surface that is bent to follow the reference trajectory and keep it along the center

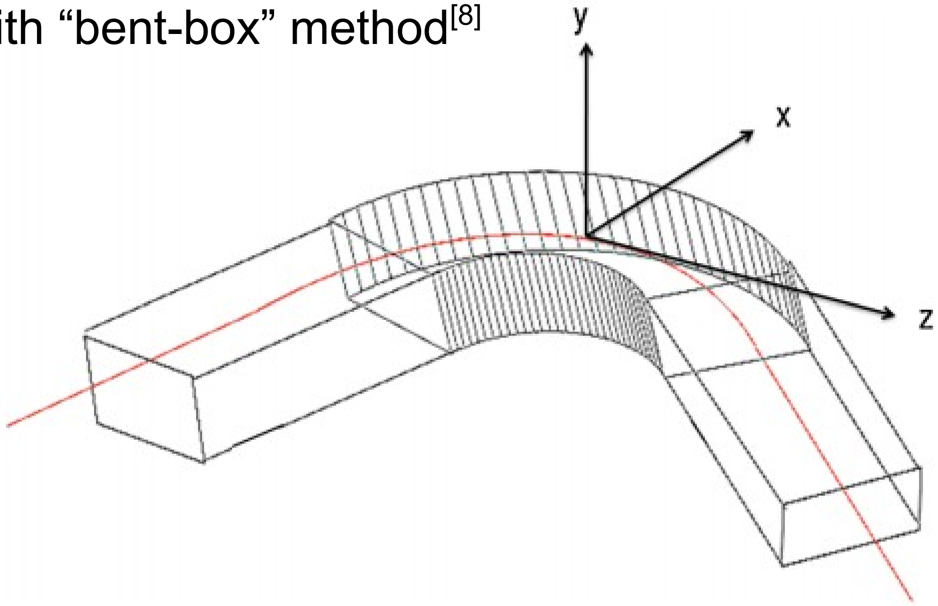


[8] C. E. Mitchell. "Calculation of Realistic charged-particle transfer maps." PhD thesis, Univ. of Maryland, College Park (2007).

# One fix is to expand field about reference orbit

- Boundary techniques of generalized gradients can be extended with “bent-box” method[8]

Normal component of B — Magnetic potential

$$\boldsymbol{A}(\boldsymbol{r}) = \int_{\partial V} dS' \; \{[\hat{\boldsymbol{n}}(\boldsymbol{r}') \cdot \boldsymbol{B}(\boldsymbol{r}')]\boldsymbol{G}^n[\boldsymbol{r}'; \boldsymbol{r}, \hat{\boldsymbol{m}}(\boldsymbol{r}')] + \psi(\boldsymbol{r}')\boldsymbol{G}^t[\boldsymbol{r}; \boldsymbol{r}', \hat{\boldsymbol{n}}(\boldsymbol{r}')]\}$$

$$\frac{\boldsymbol{m}(\boldsymbol{r}') \times (\boldsymbol{r} - \boldsymbol{r}')}{4\pi\,|\boldsymbol{r} - \boldsymbol{r}'| - \hat{\boldsymbol{m}}(\boldsymbol{r}') \cdot (\boldsymbol{r} - \boldsymbol{r}')} \qquad \frac{\hat{\boldsymbol{n}}(\boldsymbol{r}') \times (\boldsymbol{r} - \boldsymbol{r}')}{4\pi\,|\boldsymbol{r} - \boldsymbol{r}'|^3}$$

  - First envisioned as employing a bounding surface that is bent to follow the reference trajectory and keep it along the center
  - Works equally well with a curved orbit enclosed by a rectangular boundary

45 degree dipole in APS PAR

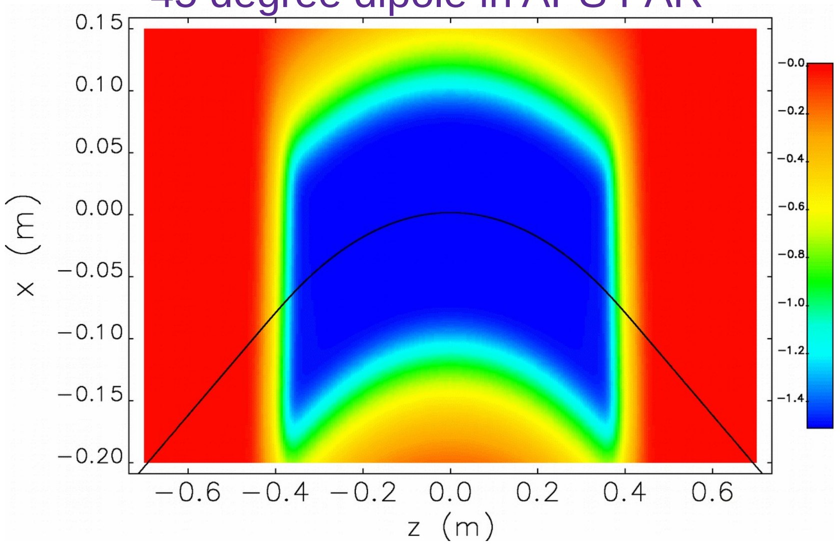


[8] C. E. Mitchell. “Calculation of Realistic charged-particle transfer maps.” PhD thesis, Univ. of Maryland, College Park (2007).

# One fix is to expand field about reference orbit

- Boundary techniques of generalized gradients can be extended with “bent-box” method[8]

Normal component of B  Magnetic potential

$$\boldsymbol{A}(\boldsymbol{r}) = \int_{\partial V} dS' \; \{[\hat{\boldsymbol{n}}(\boldsymbol{r}') \cdot \boldsymbol{B}(\boldsymbol{r}')]\boldsymbol{G}^n[\boldsymbol{r}'; \boldsymbol{r}, \hat{\boldsymbol{m}}(\boldsymbol{r}')] + \psi(\boldsymbol{r}')\boldsymbol{G}^t[\boldsymbol{r}; \boldsymbol{r}', \hat{\boldsymbol{n}}(\boldsymbol{r}')]\}$$

$$\frac{\boldsymbol{m}(\boldsymbol{r}') \times (\boldsymbol{r} - \boldsymbol{r}')}{4\pi\,|\boldsymbol{r} - \boldsymbol{r}'| - \hat{\boldsymbol{m}}(\boldsymbol{r}') \cdot (\boldsymbol{r} - \boldsymbol{r}')} \qquad \frac{\hat{\boldsymbol{n}}(\boldsymbol{r}') \times (\boldsymbol{r} - \boldsymbol{r}')}{4\pi\,|\boldsymbol{r} - \boldsymbol{r}'|^3}$$

  - First envisioned as employing a bounding surface that is bent to follow the reference trajectory and keep it along the center
  - Works equally well with a curved orbit enclosed by a rectangular boundary
- Analytic expressions for $\mathbf{A}$ and its derviatives are obtained by Taylor expanding about the reference trajectory
- While conceptually the same as the previous generalized gradient method, its numerical implementation is different

45 degree dipole in APS PAR

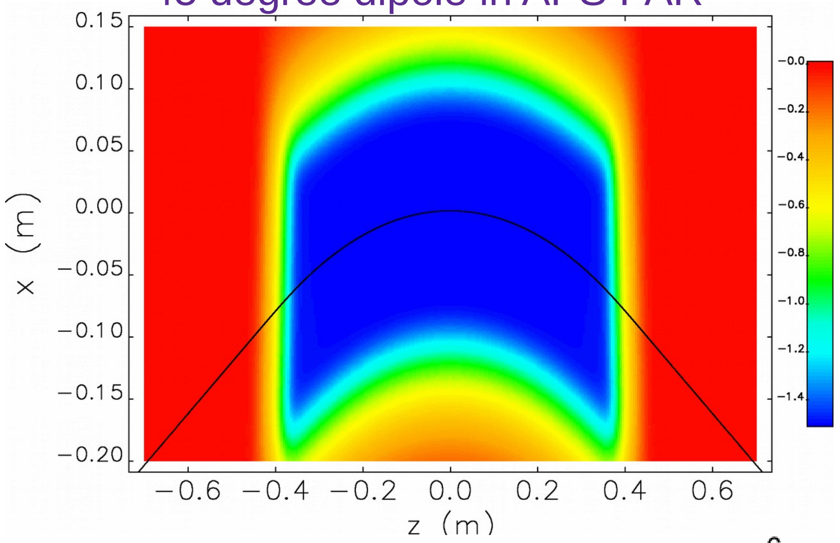


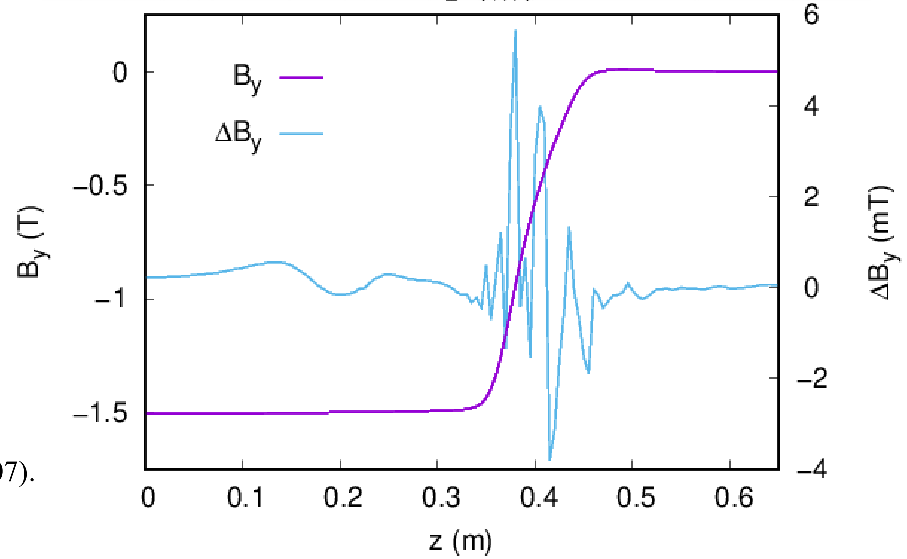


[8] C. E. Mitchell. “Calculation of Realistic charged-particle transfer maps.” PhD thesis, Univ. of Maryland, College Park (2007).

# One fix is to expand field about reference orbit

- Boundary techniques of generalized gradients can be extended with “bent-box” method[8]

Normal component of B    Magnetic potential

$$\boldsymbol{A}(\boldsymbol{r}) = \int_{\partial V} dS' \; \{[\hat{\boldsymbol{n}}(\boldsymbol{r}')\cdot\boldsymbol{B}(\boldsymbol{r}')]\boldsymbol{G}^n[\boldsymbol{r}';\boldsymbol{r},\hat{\boldsymbol{m}}(\boldsymbol{r}')] + \psi(\boldsymbol{r}')\boldsymbol{G}^t[\boldsymbol{r};\boldsymbol{r}',\hat{\boldsymbol{n}}(\boldsymbol{r}')]\}$$

$$\boldsymbol{G}^n = \frac{\boldsymbol{m}(\boldsymbol{r}')\times(\boldsymbol{r}-\boldsymbol{r}')}{4\pi\,|\boldsymbol{r}-\boldsymbol{r}'| - \hat{\boldsymbol{m}}(\boldsymbol{r}')\cdot(\boldsymbol{r}-\boldsymbol{r}')} \qquad \boldsymbol{G}^t = \frac{\hat{\boldsymbol{n}}(\boldsymbol{r}')\times(\boldsymbol{r}-\boldsymbol{r}')}{4\pi\,|\boldsymbol{r}-\boldsymbol{r}'|^3}$$

  - First envisioned as employing a bounding surface that is bent to follow the reference trajectory and keep it along the center
  - Works equally well with a curved orbit enclosed by a rectangular boundary
- Analytic expressions for $\mathbf{A}$ and its derviatives are obtained by Taylor expanding about the reference trajectory
- While conceptually the same as the previous generalized gradient method, its numerical implementation is different
- It will be interesting to compare this method of symplectic tracking with that proposed in[5]
  - Expands the Hamiltonian in both coordinates and moments
  - Uses different formulation of B-field in toroidal coordinates

45 degree dipole in APS PAR

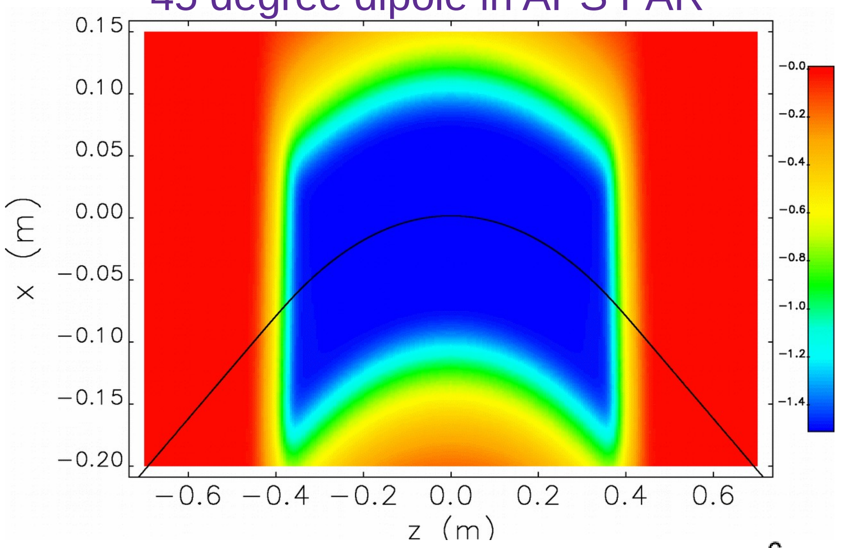


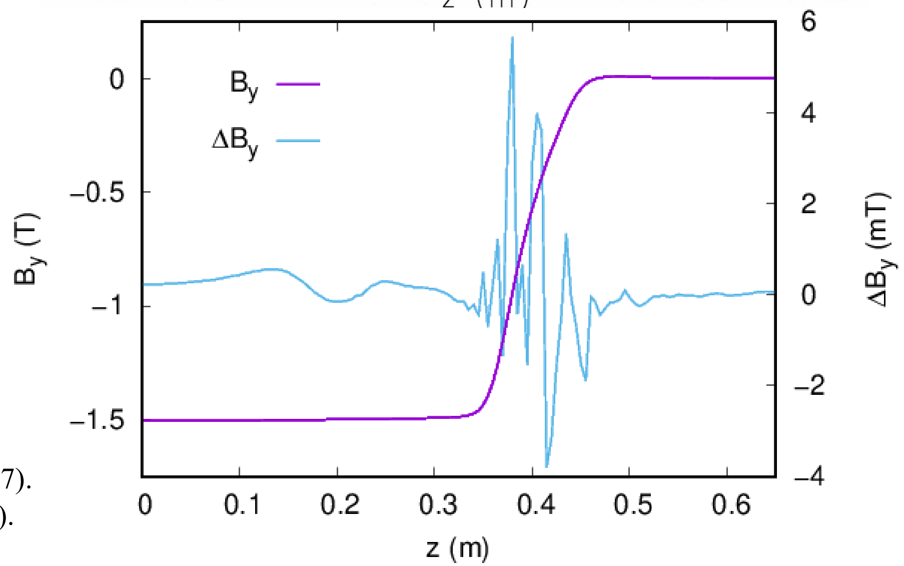



[8] C. E. Mitchell. “Calculation of Realistic charged-particle transfer maps.” PhD thesis, Univ. of Maryland, College Park (2007).
[5] A. Wolski and A.T. Herrod, “Explicit symplectic integrator...with curved reference trajectory,” PRST-AB **21**, 084001 (2018).

# Summary and future directions

- The generalized gradient representation is appealing for accelerator modeling
  - Field is represented as a Taylor series in the transverse coordinates
  - Field is divergence free and suitable for symplectic tracking
- Generalized gradients can be accurately computed from magnetic field data
  - Data can be from simulations or measurements
  - Data can be on rectangular prisms or circular cylinders
- We provide convenient tools to compute the generalized gradients for `elegant` particle tracking
- We have used generalized gradients for a variety of APS-U modeling tasks
  - Evaluation of effects of leakage fields of a Lambertson septum
  - Verification of nonlinear dynamics and emittance
  - Validation of improved hard edge and fringe models for Cartesian gradient dipoles
- Plans include expanding tools to include curved surfaces
  - Generalized gradient models of dipoles with large bending angles
  - Fringe field modeling for transverse gradient sector bends

# Extra slides

# Magnetic boundary data define the generalized gradients

- Published computational techniques use the normal component of $\boldsymbol{B}$ on a generalized cylinder[5,6,7]
  - Orthogonal functions define bases in circular, elliptical, and rectangular cylinder
  - Solutions converge rapidly and also smooth any noise/errors in the boundary data
    - GG-”true solution” is a harmonic function whose maximum must lie on the boundary
- If the field has $B_z \neq 0$ on-axis (solenoidal component), we found that $B_z$ on the boundary is also needed

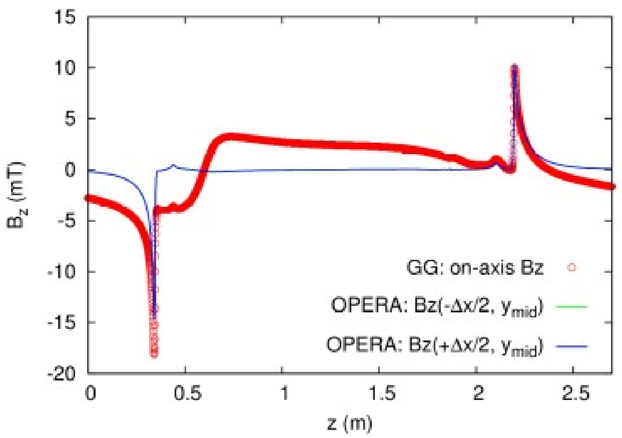


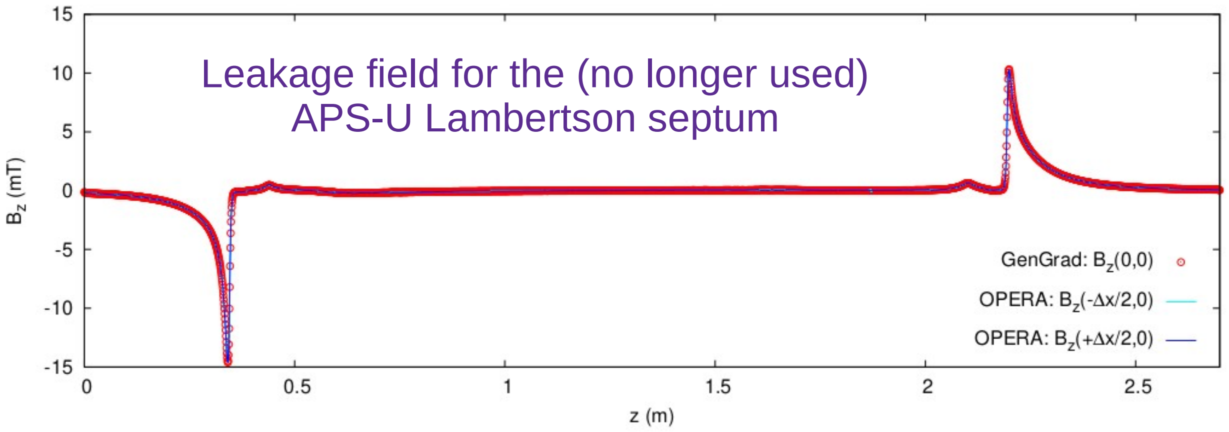

# Application to modeling the septum leakage field

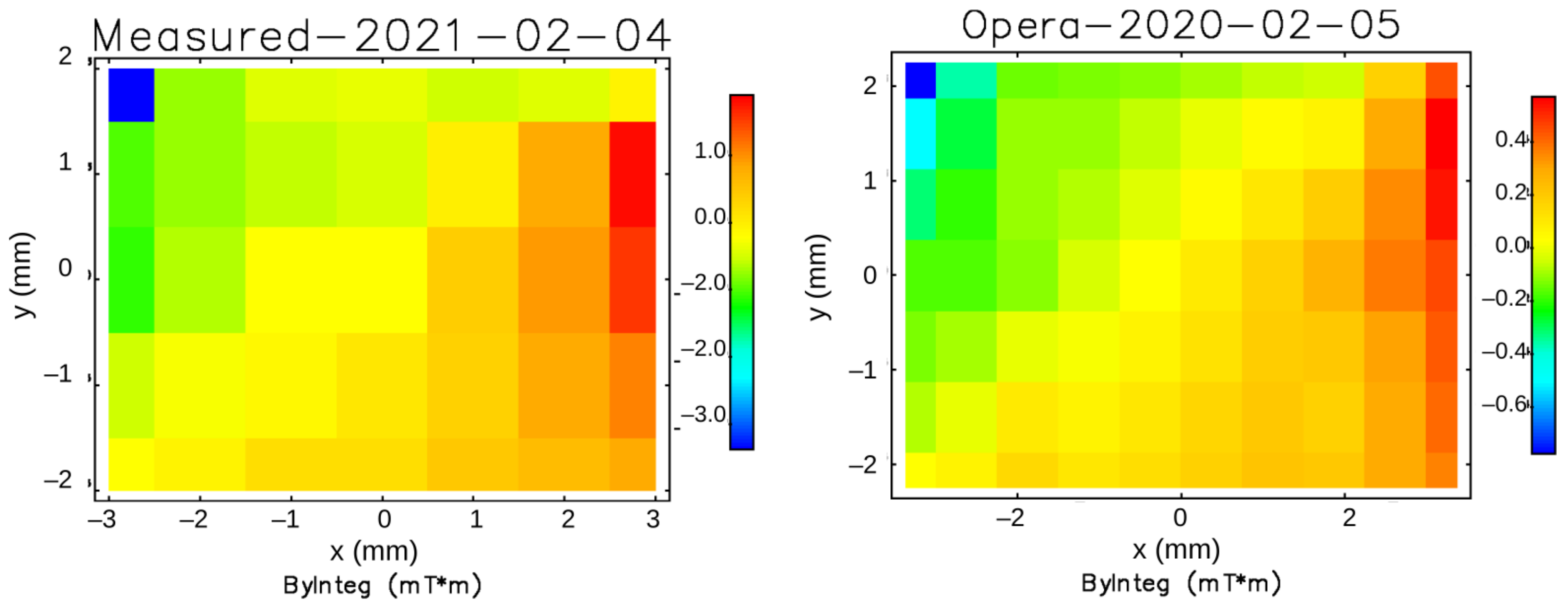


- Prototype APS-U Lambertson septum magnet[18] was built by FNAL and measured in May 2021
- Measurements by M. Kasa, *et al.* showed similar field map profiles to simulations, but with integrated leakage fields ~4 times larger than simulation predicted (error in construction)
- Previous studies indicated that a leakage field of this size could reduce injection efficiency and lifetime[19]
- We studied this issue using a generalized gradient field model derived from measurements

[18] M. Abliz *et al*. “A concept for canceling the leakage field inside the stored beam chamber of a septum magnet” NIM A **886**, 7 (2017).
[19] A. Xiao et al. Private communication.

# Generalized gradient expansion (GGE) shows some deviations from the field measurements

- `computeRBGGE` found optimal "fit" using 6 multipoles and 2 derivatives
  - Rms "fit" error is 9X the 83 μT  measurement error
- On-axis $B_y$ and $B_z$ match well, but $B_x$ does not
- Field differences appear in all components off axis

| Component | RMS error | Largest error |
|---|---|---|
| $\Delta B_x$ | 0.55 mT | 5.84 mT |
| $\Delta B_y$ | 0.41 mT | 4.72 mT |
| $\Delta B_z$ | 0.20 mT | 6.88 mT |

- Inserting `BGGEXP` model into the APS-U lattice shows no significant harmful effects
  - Prior results based on kickmaps appear to have been misleading

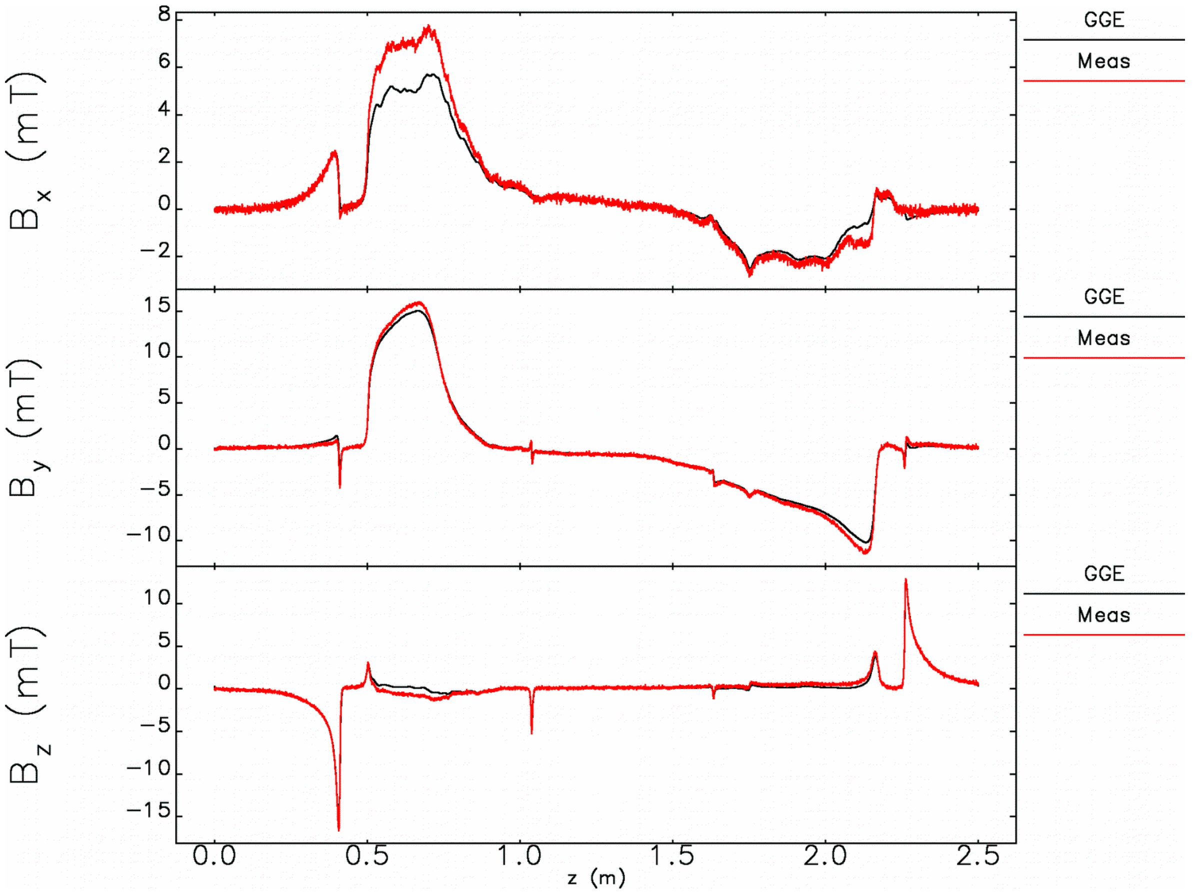

# Generalized gradient expansion (GGE) shows some deviations from the field measurements

- `computeRBGGE` found optimal "fit" using 6 multipoles and 2 derivatives
  - Rms "fit" error is 9X the 83 μT measurement error
- On-axis $B_y$ and $B_z$ match well, but $B_x$ does not
- Field differences appear in all components off axis

| Component | RM |
|---|---|
| $\Delta B$ | |
| $\Delta$ | |
| $\Delta B$ | |

- Inserting … the APS-U lattice shows no … harmful effects
  - Prior results based on kickmaps appear to have been misleading

We have since changed injection schemes, so Lambertson septum is no longer needed.

Presently, we are working to convert measured undulator magnetic field data into a generalized gradient representation for tracking.

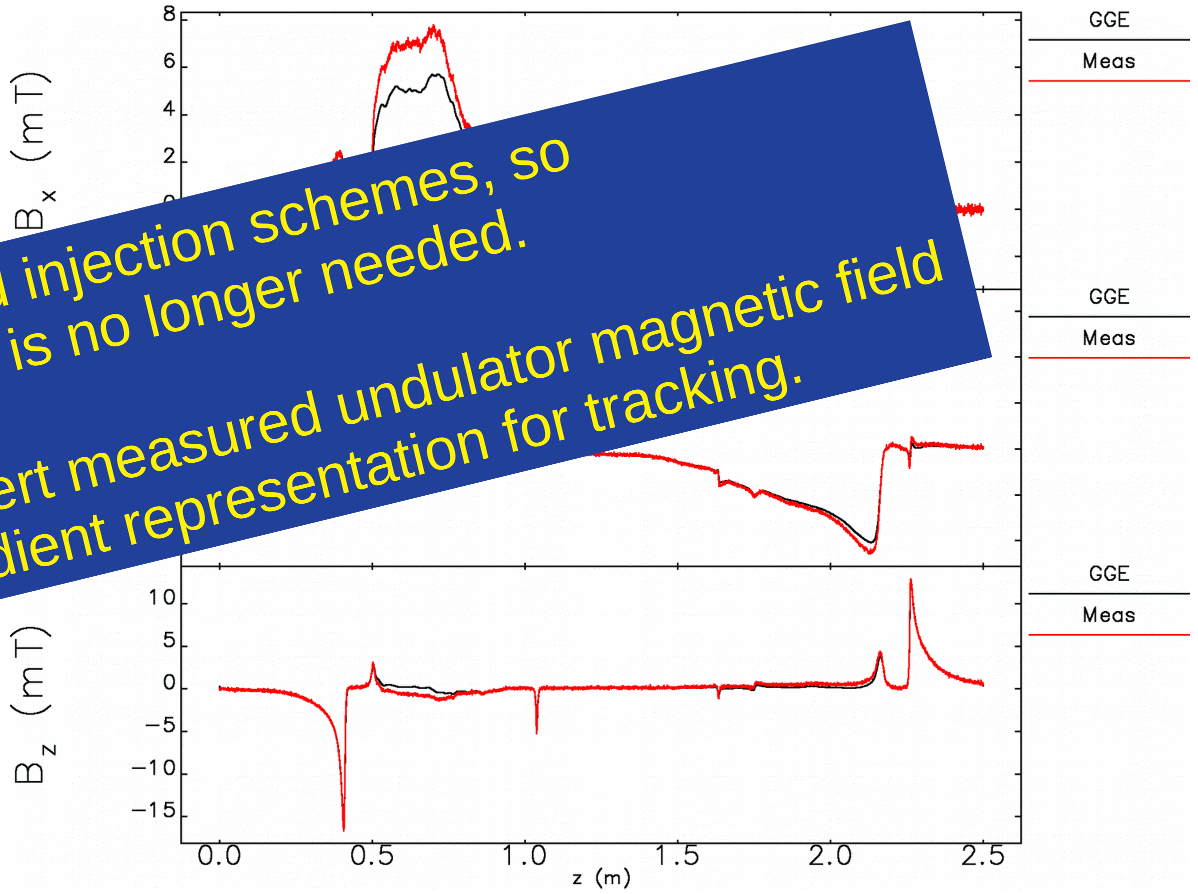

# GGE and usual tracking respond similarly to errors

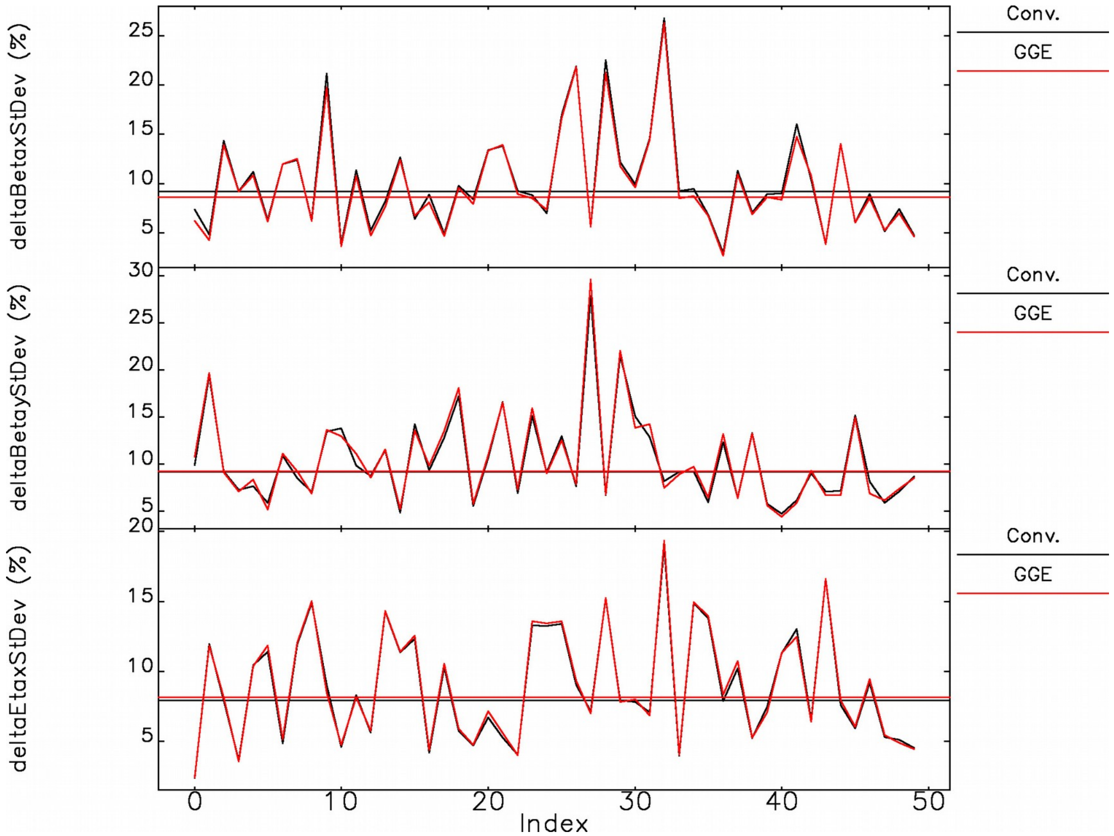


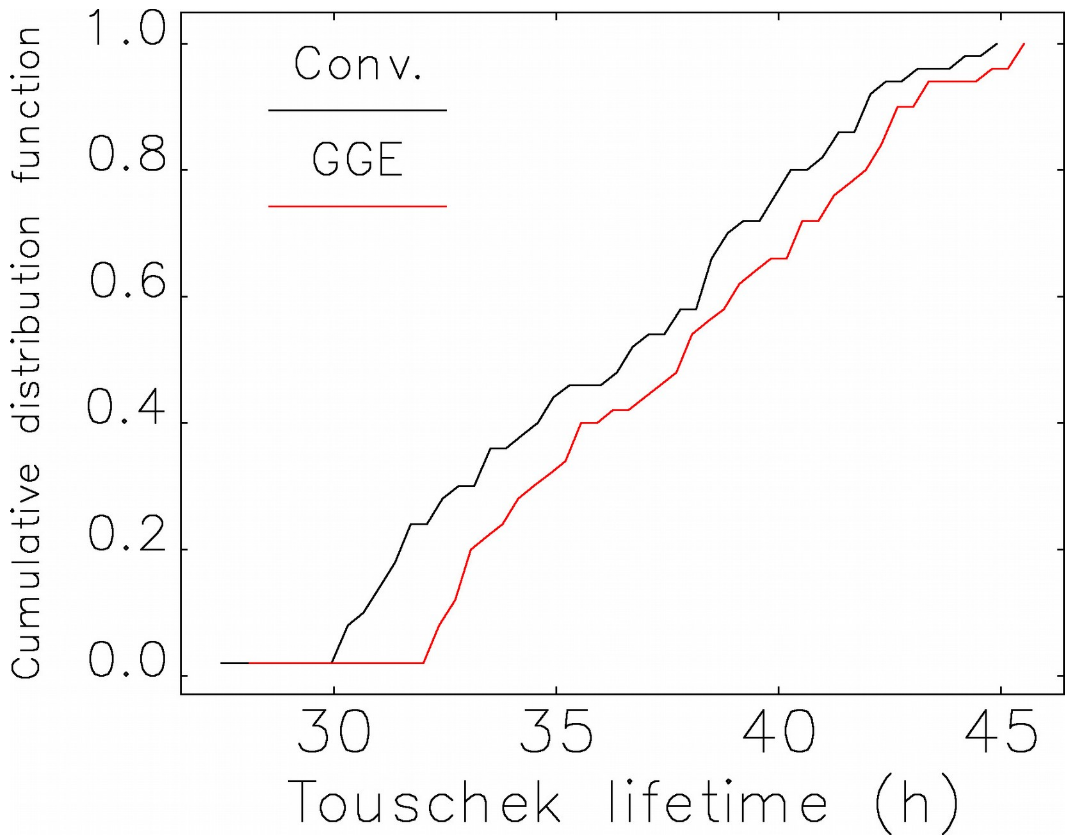


- Adding 30 micron rms misalignments to all sextupoles results in very similar lattice beating
- Computed the local momentum acceptance using 1000 turns for 50 instances of each case
- Resulting Touschek lifetimes differ by less than 8%, assuming $\varepsilon_x = \varepsilon_y = 30$ pm, $\sigma_\delta = 0.12\%$, $\sigma_t = 100$ ps
  - Note: direct tracking using large sextupole offsets to model errors would result in a larger emittance

# GGE model confirms APS-U emittance

- Ultra-low emittance is a key deliverable for the APS-U
- The implementation of `BGGEXP` includes synchrotron emission
- Tracking of 1,000 particles, averaged over 5,000 turns:
  - Emittance = 41.0 pm ☺
  - Energy spread = 0.127% ☺
  - 48,000 core hours (!)
- Diffusion matrix computation takes ~200 core hours, and gives essentially identical results

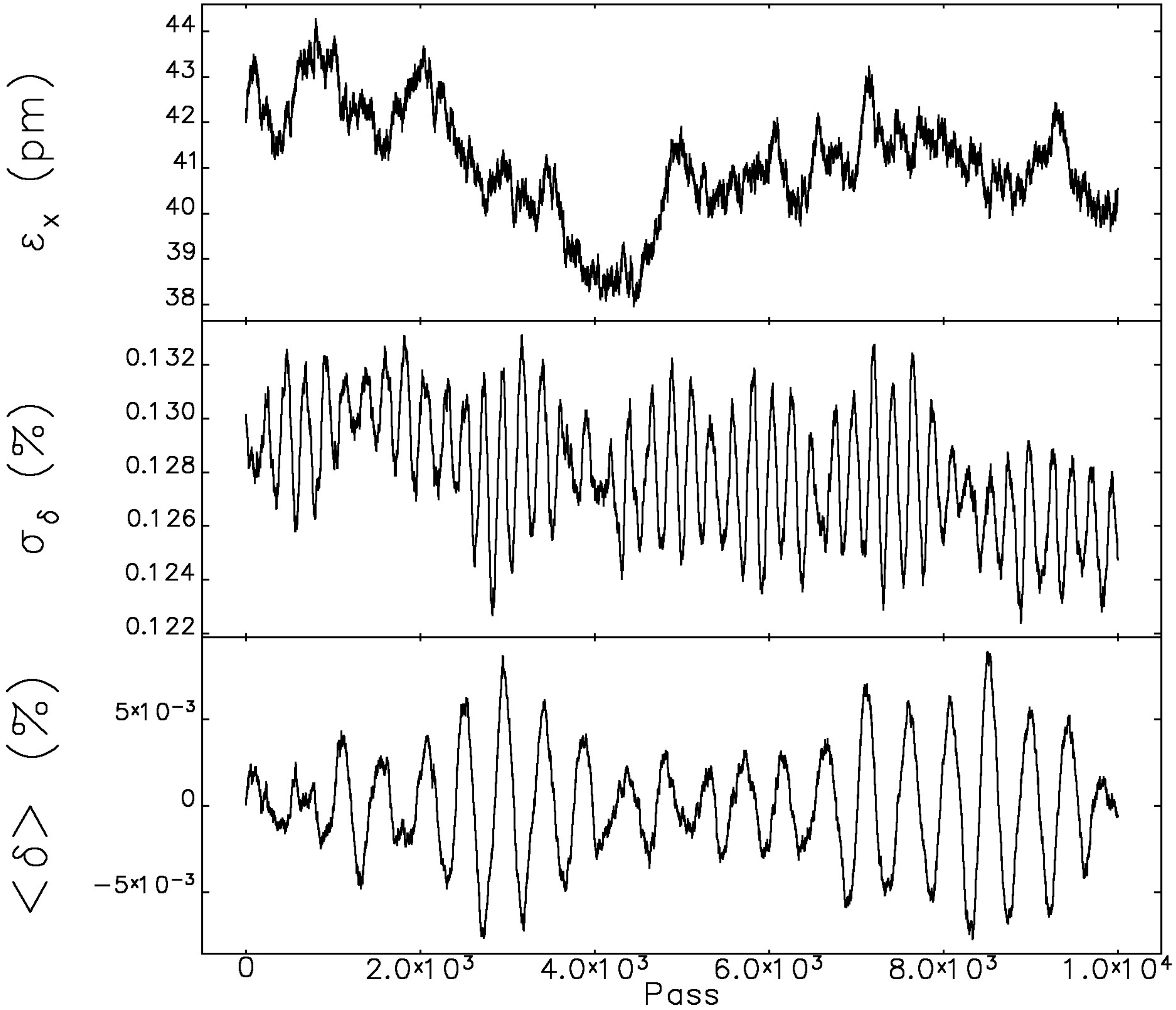

# A hard edge model of more complicated magnets

- The field in the hard edge magnet only depends on the transverse coordinates
  - Fields have unambiguous description in terms of multipole components
  - Tracking with explicit, symplectic integrators is possible using splitting methods
- The difference between the dynamics within the hard edge model and that in the actual magnetic field is collected under the umbrella of "fringe field" effects
- We define the hard edges such that the integrated bending field of the model matches the real magnet:

$$\int_{z_-}^{z_+} dz\, B_y(0,0,z) = \int_{z_-}^{z_+} dz\, C_1(z) = (z_+ - z_{\text{edge}})C_1(z_+) + (z_{\text{edge}} - z_-)C_1(z_-) = (z_+ - z_{\text{edge}})\frac{p_0}{q}\frac{1}{\rho_+} + (z_{\text{edge}} - z_-)\frac{p_0}{q}\frac{1}{\rho_-}$$

Magnet entrance:

- Bending radii $\rho_+ = \rho$, while $\rho_- \to \infty$
- Endpoints $z_- \to -\infty$, while $z_+$ at peak $|B_y|$

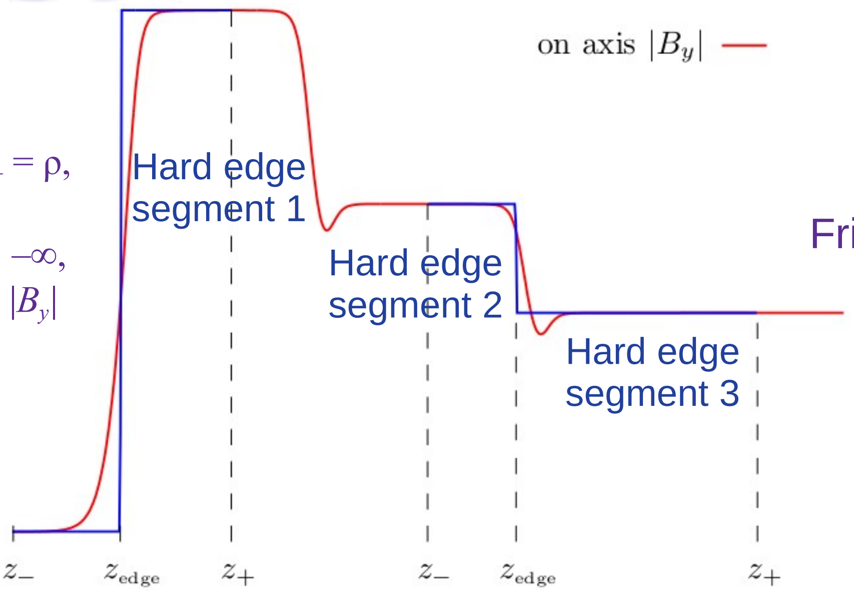


Multipole content is defined by the on-axis gradient + hard edges

Fringe between segments:

- Non-zero bending radii $\rho_+$ and $\rho_-$ both upstream and downstream
- Endpoints $z_\pm$ near the center of the flat-field region
- Fringe field is "more interesting"

# Linear matrix element comparisons using the improved fringe field model for the Q4

CCBEND model[19] but with no fringe effects

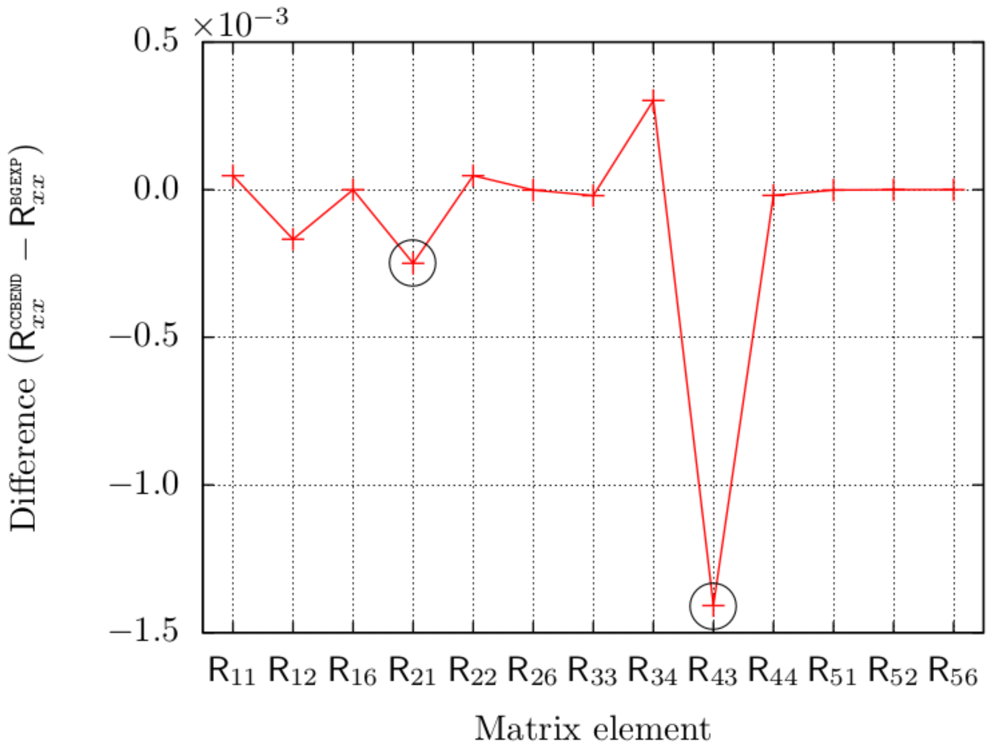


“Complete” CCBEND model with fringe effects

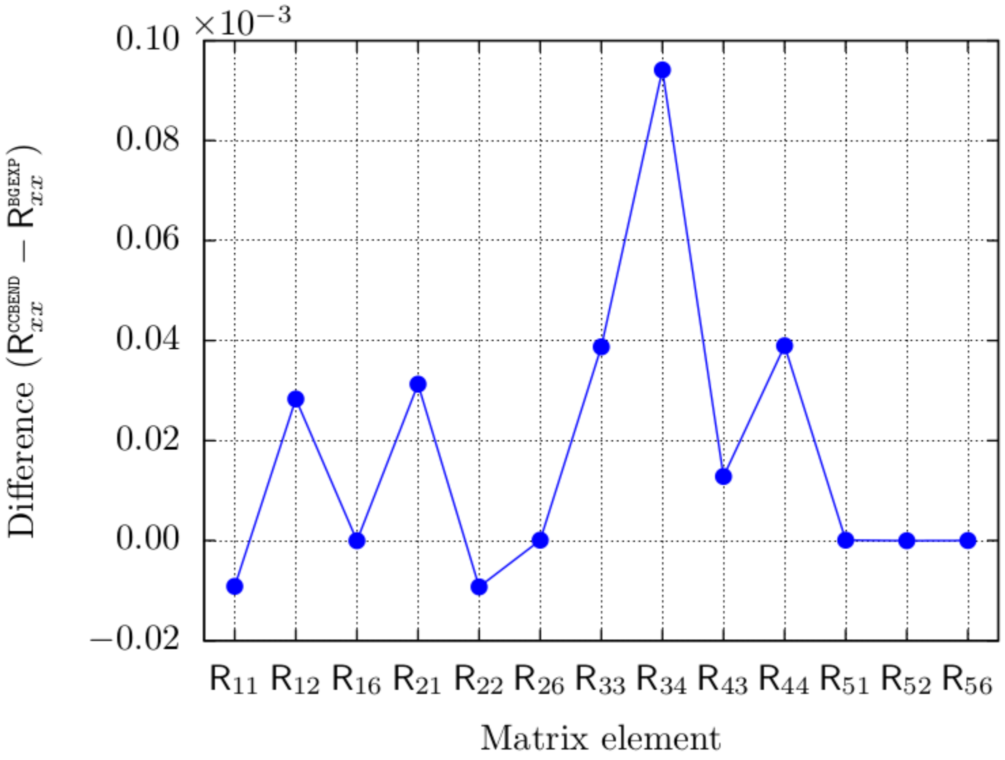


- Linear matrix elements of the hard edge model differ from GGE tracking by < 0.15%
- Improved fringe theory reduces differences in the linear matrix elements to the few x $10^{-5}$ level or better
- Hard edge model has “too much” focusing in both horizontal and vertical planes

[20] M. Borland, “Symplectic Integration in elegant,” Tech. Rep.LS-356, Advanced Photon Source, 2021.

# Improved accuracy of the Q4 fringe field model is required to obtain good tune predictions

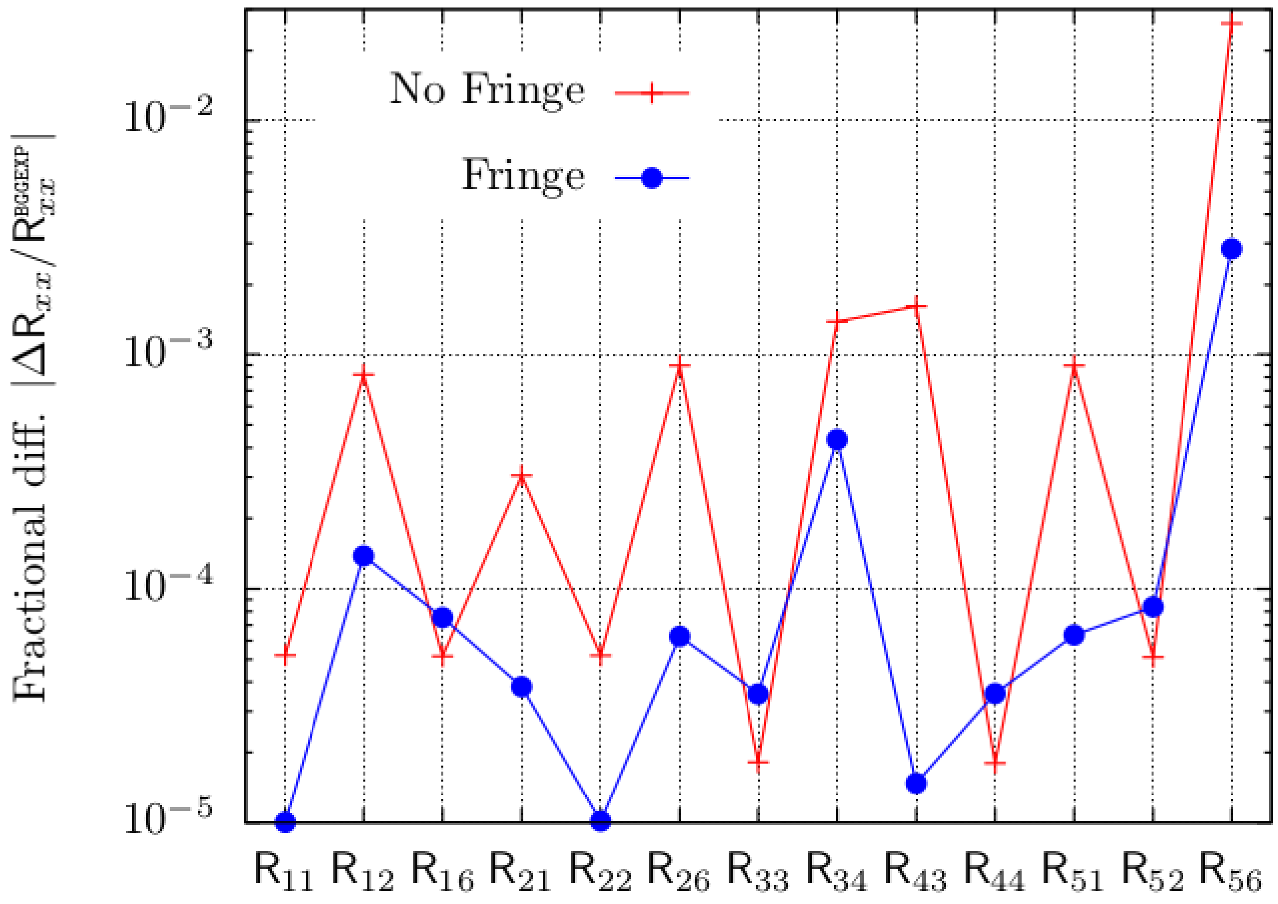


- Fractional error in the linear matrix elements are
  - ~ 0.1% without fringe contributions
  - ~ 0.02% including fringe terms
- Tunes are sensitive to the focusing in Q4 reverse bend due to its large beta function
- Are these models good enough for accurate modeling of the APS-U lattice?
  - Comparison of tunes shows very good agreement with fringe model included

| Model | $\nu_x$ | $\nu_x$ |
|---|---|---|
| **No Fringe** | **95.0038** | **36.1560** |
| **Fringe** | **94.9832** | **36.0872** |
| **BGGEXP** | **94.9856** | **36.0878** |

We feel reasonably confident that we are accurately modeling our transverse gradient reverse bends

# Very good results are found for both Q4 and Q5

| Model | $\beta_x$ (m) | $\beta_y$ (m) | $\eta_x$ (mm) | $\nu_x$ | $\nu_x$ | $\xi_x$ | $\xi_y$ |
|---|---|---|---|---|---|---|---|
| BGGEXP Q5 | 5.220 | 2.406 | 0.3938 | 95.116 | 36.076 | –133.95 | –111.39 |
| CCBEND Q5 | 5.219 | 2.406 | 0.3936 | 95.115 | 36.076 | –133.94 | –111.39 |
| BGGEXP Q4 | 5.071 | 2.398 | 0.3507 | 94.986 | 36.088 | –131.45 | –111.79 |
| CCBEND Q4 | 5.068 | 2.399 | 0.3471 | 94.983 | 36.087 | –131.41 | –111.79 |
| BGGEXP Q4+Q5 | 5.102 | 2.413 | –0.6282 | 95.001 | 36.064 | –132.09 | –111.55 |
| CCBEND Q4+Q5 | 5.085 | 2.414 | 0.4601 | 94.998 | 36.063 | –131.68 | –111.55 |

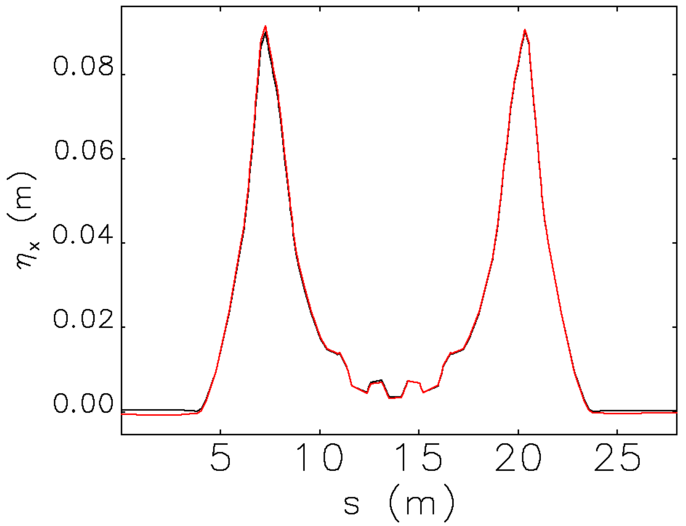


- Tunes agree to within 0.003 for all cases
- For models that just replace the Q4 or Q5 we have
  - Linear lattice function agreement to better than 1%
  - Chromaticities that are essentially identical
- Agreement of lattice functions and chromaticies are somewhat worse when we replace both Q4 & Q5
  - I assume that this is because both are essentially on the integer $\nu_x$ resonance, but we'll see…

# Generalized gradient tracking has verified a new model of our longitudinal gradient dipole

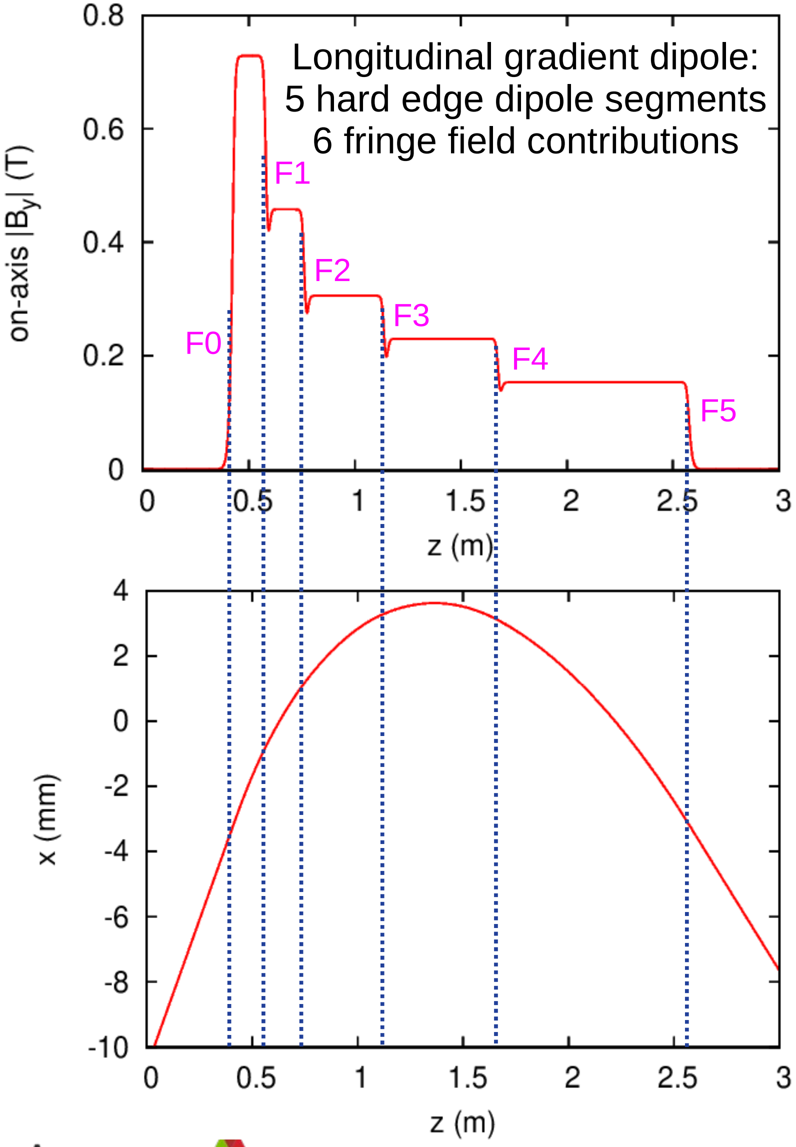


- Hard edges are set to match integrating bending field
- Fringe field maps defined by (actual field) – (hard edge field)

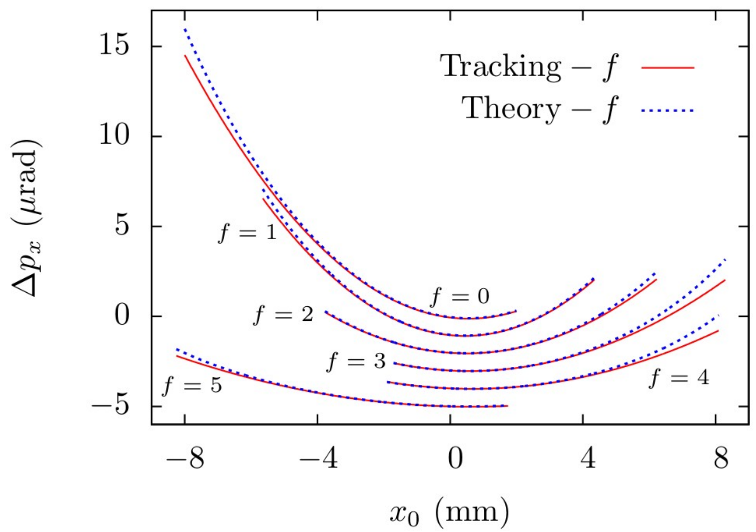


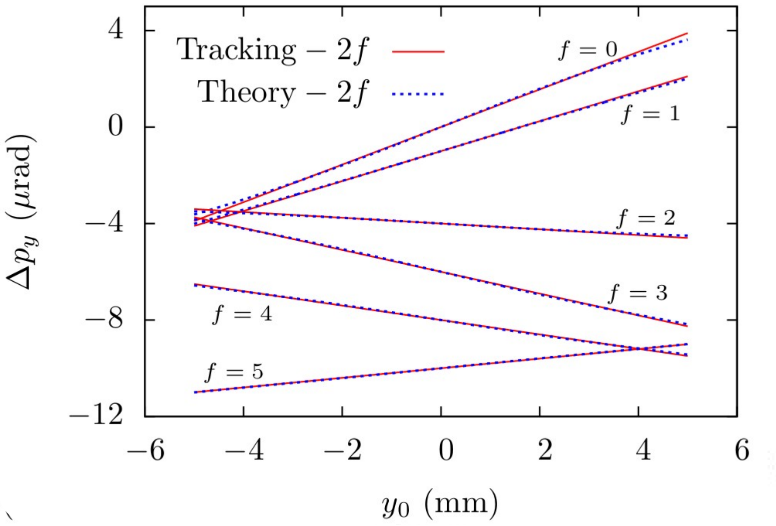


Linear matrix from generalized gradient tracking (`BGGEXP`)

$$\begin{bmatrix} 0.99822 & 2.2243 & 0 & 0 & 0 & 0.04035 \\ -0.00101 & 0.9995 & 0 & 0 & 0 & 0.02857 \\ 0 & 0 & 1.0009 & 2.2251 & 0 & 0 \\ 0 & 0 & 0.00051 & 1.0002 & 0 & 0 \\ 0.02856 & 0.0232 & 0 & 0 & 1 & 0.00029 \\ 0 & 0 & 0 & 0 & 0 & 1 \end{bmatrix}$$

Linear matrix from the new, hard-edge `LGBEND` element

$$\begin{bmatrix} 0.99816 & 2.2242 & 0 & 0 & 0 & 0.04029 \\ -0.00106 & 0.9995 & 0 & 0 & 0 & 0.02857 \\ 0 & 0 & 1.0010 & 2.2253 & 0 & 0 \\ 0 & 0 & 0.00056 & 1.0003 & 0 & 0 \\ 0.02856 & 0.0233 & 0 & 0 & 1 & 0.00029 \\ 0 & 0 & 0 & 0 & 0 & 1 \end{bmatrix}$$